CRISPR screens identify genomic ribonucleotides as a source of PARP-trapping lesions

Michal Zimmermann[#1], **Olga Murina**[#2], **Martin A. M. Reijns**[2], **Angelo Agathanggelou**[3], **Rachel Challis**[2], **Žygimant Tarnauskait**[2], **Morwenna Muir**[4], **Adeline Fluteau**[2], **Michael Aregger**[5], **Andrea McEwan**[1], **Wei Yuan**[6], **Matthew Clarke**[6], **Maryou B. Lambros**[6], **Shankara Paneesha**[7], **Paul Moss**[8], **Megha Chandrashekhar**[5,9], **Stephane Angers**[10], **Jason Moffat**[5,9,11], **Valerie G. Brunton**[4], **Traver Hart**[12], **Johann de Bono**[6], **Tatjana Stankovic**[3], **Andrew P. Jackson**[2,¶], and **Daniel Durocher**[1,9,¶]

[1]The Lunenfeld-Tanenbaum Research Institute, Mount Sinai Hospital, 600 University Avenue, Toronto, ON, M5G 1X5, Canada

[2]MRC Human Genetics Unit, Institute of Genetics and Molecular Medicine, University of Edinburgh, Western General Hospital, Crewe Road South, Edinburgh EH4 2XU, UK

[3]Institute for Cancer and Genomic Sciences, University of Birmingham, Edgbaston, Birmingham, B15 2TT, UK

[4]Cancer Research UK Edinburgh Centre, University of Edinburgh, Edinburgh, EH4 2XU, UK

[5]Donnelly Centre, University of Toronto, Toronto, ON, M5S 3E1, Canada

[6]The Institute of Cancer Research, London, UK and the Royal Marsden NHS Foundation Trust, London, UK

[7]Heartlands Hospital, Bordesley Green East, Bordesley Green, Birmingham, West Midlands, B9 5SS, UK

¶Address correspondence to: Daniel Durocher, Ph.D., The Lunenfeld-Tanenbaum Research Institute, Mount Sinai Hospital, Room 1073, 600 University Avenue Toronto, ON M5G 1X5, CANADA, Tel: 416-586-4800 ext. 2544, durocher@lunenfeld.ca; Andrew P. Jackson, MRCP Ph.D., MRC Human Genetics Unit, Institute of Genetics and Molecular Medicine, University of Edinburgh, Western General Hospital, Crewe Road South, Edinburgh EH4 2XU, UK, andrew.jackson@igmm.ed.ac.uk.

Data Availability
Results of PARP inhibitor CRISPR screens, source data for mouse xenograft experiments, unprocessed images of immunoblots and examples of gating strategies for FACS experiments are provided as Supplementary Information. All other datasets generated during this study are available from the corresponding authors upon reasonable request.

[8]Institute of Immunology and Immunotherapy, University of Birmingham, Edgbaston, Birmingham, B15 2TT, UK

[9]Department of Molecular Genetics, University of Toronto, Toronto, ON, M5S 3E1, Canada

[10]Department of Pharmaceutical Sciences, Leslie Dan Faculty of Pharmacy & Department of Biochemistry, Faculty of Medicine, University of Toronto, Toronto, ON, M5S 3M2, Canada

[11]Canadian Institute for Advanced Research, Toronto, ON, M5G 1M1, Canada

[12]Department of Bioinformatics and Computational Biology, The University of Texas MD Anderson Cancer Center, Houston, TX, USA

[#] These authors contributed equally to this work.

Summary

The observation that BRCA1- and BRCA2-deficient cells are sensitive to poly(ADP-ribose) polymerase (PARP) inhibitors spurred their development into cancer therapies that target homologous recombination (HR) deficiency1. The cytotoxicity of PARP inhibitors depends on PARP trapping, the formation of non-covalent protein-DNA adducts composed of inhibited PARP1 bound to DNA lesions of unclear origins1–4. To address the nature of such lesions and the cellular consequences of PARP trapping, we undertook three CRISPR screens to identify genes and pathways that mediate cellular resistance to olaparib, a clinically approved PARP inhibitor1. Here were present a high-confidence set of 73 genes whose mutation causes increased PARP inhibitor sensitivity. In addition to an expected enrichment for HR-related genes, we discovered that mutation in all three genes encoding RNase H2 sensitized cells to PARP inhibition. We establish that the underlying cause of the PARP inhibitor hypersensitivity of RNase H2-deficient cells is impaired ribonucleotide excision repair (RER)5. Embedded ribonucleotides, abundant in the genome of RER-deficient cells, are substrates for topoisomerase 1 cleavage, resulting in PARP-trapping lesions that impede DNA replication and endanger genome integrity. We conclude that genomic ribonucleotides are a hitherto unappreciated source of PARP-trapping DNA lesions, and that the frequent deletion of *RNASEH2B* in metastatic prostate cancer and chronic lymphocytic leukemia could provide an opportunity to exploit these findings therapeutically.

We carried out dropout CRISPR screens with olaparib in three cell lines of diverse origins, representing both neoplastic and non-transformed cell types (Fig 1a and ED Fig 1a,b). The cell lines selected were HeLa, derived from a human papilloma virus-induced cervical adenocarcinoma; RPE1-hTERT, a telomerase-immortalized retinal pigment epithelium cell line; and SUM149PT, originating from a triple-negative breast cancer with a hemizygous *BRCA1* mutation6. SUM149PT cells express a partially defective BRCA1 protein (BRCA1-11q)7 and thus provided a sensitized background to search for enhancers of PARP inhibition cytotoxicity in HR-compromised cells. The screens were performed in technical triplicates, and a normalized depletion score for each gene was computed using DrugZ8. To identify high-confidence hits, we used a stringent false discovery rate (FDR) threshold of 1%. To this initial list, we added genes that were found at an FDR threshold of <10% in at least two cell lines. This analysis identified 64, 61 and 116 genes whose inactivation caused

sensitization to olaparib in the HeLa, RPE1-hTERT and SUM149PT cell lines, respectively, giving a total of 155 different genes (Supplementary Table 1).

Out of this list, 13 genes scored positive in all three cell lines and a further 60 genes were common to two cell lines, which we combine to define a core set of 73 high-confidence PARP inhibitor (PARPi)-resistance genes (Fig 1b and Supplementary Table 1). Gene ontology analysis of the 73- and 155-gene sets (Fig 1c and ED Fig 1c, respectively) shows strong enrichment for HR-related biological processes, providing unbiased confirmation that the screens identified bona fide regulators of the response to PARP inhibition. Mapping the 73-gene set on the HumanMine protein-protein interaction data (Fig 1d) generated a highly connected network consisting of DNA damage response genes that include many HR regulators (such as *BRCA1*, *BARD1*, *BRCA2* and *PALB2*), components of the Fanconi anemia pathway, as well as the kinases *ATM* and *ATR*. Outside or at the edge of the network, we noted the presence of genes encoding the MUS81-EME1 nuclease, splicing and general transcription factors (such as SF3B3/5 and CTDP1) and the three genes coding for the RNase H2 enzyme complex (*RNASEH2A*, *RNASEH2B* and *RNASEH2C*). *RNASEH2A/B/C* were hits in all three cell lines, with *RNASEH2A* and *B* being the two highest-scoring genes, as determined by the mean DrugZ value from the three cell lines (Supplementary Table 1). A similar analysis of the 155-gene set generated an even denser network, with additional genes lying at the periphery of an HR and Fanconi anemia core (ED Fig 1d).

Next, we generated RNase H2-null HeLa, RPE1, SUM149PT and HCT116 clonal cell lines using genome editing (denoted as *KO*; ED Fig 2a-d) and confirmed that RNase H2 deficiency caused hypersensitivity to both olaparib and a second clinical-stage PARPi, talazoparib, in all cell lines tested (Fig 2a,b and ED Fig 2e-g, with EC50 values reported in ED Fig. 2h). The *RNASEH2A/B-KO* cells also exhibited elevated levels of apoptosis after PARP inhibition (ED Fig 2i-l), a phenotype that was particularly prominent with talazoparib treatment (ED Fig 2i-l). Given the strength of the PARPi-induced phenotypes in RNase H2-deficient cells, and since RNase H2 had not been previously linked to the response to PARP inhibition, we sought to determine the mechanism of PARPi sensitization in RNase H2-deficient cells.

Since HR deficiency causes PARPi sensitivity, we first considered that RNase H2 might promote HR. Consistent with this possibility, fission yeast cells that combine mutations in RNase H2 and RNase H1 are HR-defective[9]. However, in RNase H2-deficient cells, RAD51 readily formed ionizing radiation-induced foci, suggesting efficient recombinase filament assembly (Fig 2c,d and ED Fig 3a,b). Furthermore, HR efficiency, as assessed by the direct repeat (DR)-GFP assay[10], was at near wild-type levels in cells transduced with *RNASEH2A* and *RNASEH2B* sgRNAs (Fig 2e and ED Fig 3c,d). Thirdly, rather than reduced HR, *RNASEH2A-KO* cells displayed higher levels of sister chromatid exchanges, reminiscent of the 'hyper-rec' phenotype observed in RNase H2-deficient yeast[11] (Fig 2f). This phenotype was likely due to elevated levels of replication-dependent DNA damage, as determined by γ-H2AX staining (Fig 2g and ED Fig 3e-h) and marked poly(ADP-ribosylation) of PARP1 (Fig 2h and ED Fig 3i,j), supporting previous observations of replication-associated genome instability in yeast and mammalian cells deficient in RNase H2[12–14].

The increased levels of sister chromatid exchanges prompted us to test if RNase H2-deficient cells required HR for survival. Indeed, we observed synthetic lethality when an sgRNA against *RNASEH2B* was delivered into engineered *BRCA1-KO* and *BRCA2-KO* cell lines in the RPE1-hTERT and DLD-1 backgrounds, respectively (Fig 2i and ED Fig 3k-o).

RNase H2 cleaves single ribonucleotides incorporated into DNA, as well as longer RNA:DNA hybrids15. To distinguish between these two functions, we carried out cellular complementation experiments with variants of RNase H2. The sensitivity of *RNASEH2A-KO* cells to olaparib was not rescued by either a catalytically-inactive RNase H2 enzyme (RNASEH2A D34A/D169A), or by a separation-of-function mutant (RNASEH2A P40D/Y210A16) that retains activity against RNA:DNA hybrids, but not DNA-embedded monoribonucleotides (Fig 2j and ED Fig 4). These data indicate that it is likely the removal of genome-embedded ribonucleotides by RER, and not RNA:DNA hybrid cleavage by RNase H2, which protects cells from PARPi-induced cytotoxicity.

To determine the genetic basis of the sensitivity of *RNASEH2A-KO* cells to PARPi, we carried out CRISPR screens to identify mutations that restored resistance to talazoparib in RNase H2-deficient HeLa and RPE1-hTERT cell lines (Fig 3a, ED Fig 5a and Supplementary Table 2). The screens identified a single common gene, *PARP1*. The genetic dependency on *PARP1* for talazoparib- and olaparib-induced cytotoxicity was confirmed in double *RNASEH2A-KO/PARP1-KO* cells (Fig 3b and ED Fig 5b-e), providing evidence that the lethality associated with PARP inhibition requires formation of trapped PARP1-DNA adducts4. Consistent with this finding, treatment with veliparib, a PARP inhibitor with poor trapping ability4 induced much less apoptosis than olaparib or talazoparib in *RNASEH2A-KO* cells (ED Fig 5f).

Analysis of DNA content by flow cytometry revealed that *RNASEH2A-KO* cells arrest in S phase in a PARP1-dependent manner upon talazoparib treatment (Fig 3c and ED Fig 5g). *RNASEH2A-KO* cells also demonstrated elevated levels of talazoparib-induced γ-H2AX and these levels did not decline upon drug removal (Fig 3c and ED Fig 5h). These observations suggest that unresolved DNA lesions induced by PARP trapping are the likely cause of cell death in PARPi-treated *RNASEH2A-KO* cells.

Genome instability in RER-deficient yeast cells is dependent on an alternative, topoisomerase 1 (TOP1)-mediated ribonucleotide excision pathway18–20. In this process, TOP1 enzymatic cleavage 3' of the embedded ribonucleotide results in DNA lesions predicted to engage PARP1, including nicks with difficult-to-ligate 2'-3' cyclic phosphate ends18,19,21 and covalent TOP1-DNA adducts (TOP1 cleavage complexes22) in conjunction with single-strand DNA gaps or DSBs23. Given that the mechanisms promoting genome instability in mammalian RNase H2-deficient cells remain poorly defined, we assessed whether TOP1 action on misincorporated ribonucleotides contributed to the DNA damage observed in human RER-deficient cells. Short-term TOP1 depletion with short interfering RNAs (siRNAs) reduced the number of γ-H2AX foci in RNase H2-deficient cells to nearly wild-type levels (Fig. 3d-f and ED Fig 6a). Furthermore, TOP1-mediated ribonucleotide cleavage contributed to PARPi sensitivity, as depletion of TOP1 with

independent siRNAs in *RNASEH2A-KO* cells reduced the levels of talazoparib-induced apoptosis (Fig 3g and ED Fig 6b-e). TOP1 depletion also reduced talazoparib-induced apoptosis in the RER-deficient RNASEH2A P40D/Y210A cells (ED Fig 6f-h) and ameliorated the talazoparib-induced S-phase arrest (ED Fig 6i). Together, these results strongly suggest that the processing of genome-embedded ribonucleotides by TOP1 leads to DNA lesions that engage PARP1, creating a vulnerability to PARP trapping.

The *RNASEH2B* gene resides on chromosome 13q14 in proximity to two tumour suppressor loci. One of them, the *DLEU2-mir-15-16* microRNA cluster, is a target of 13q14 deletions observed in over 50% of chronic lymphocytic leukemia (CLL) cases[24]. As a result, collateral homozygous deletion of *RNASEH2B* can occur in CLL and other hematopoietic malignancies[25]. Additionally, in prostate cancer, frequent deletions at 13q14 involving the *RB1* but not the *BRCA2* locus[26] might also result in *RNASEH2B* loss. Such 13q14 deletions are late events associated with endocrine therapy resistance, luminal-to-basal phenotype transition and rapid disease progression[27,28].

We determined *RNASEH2B* copy number by multiplex ligation-dependent probe amplification (MLPA) in 100 CLL patients. *RNASEH2B* deletions were present in 43% of CLL samples, with biallelic loss detected in 14%. Co-deletion of the *DLEU2* microRNA cluster was confirmed by CGH microarray (Fig 4a and ED Fig 7a,b), establishing that collateral *RNASEH2B* loss is frequent in CLL. Furthermore, analysis of whole-exome sequencing of metastatic castration-resistant prostate cancers[29] demonstrated frequent collateral loss of *RNASEH2B* with *RB1* gene deletion co-occurring in 34% of tumours (2% biallelic loss; ED Fig 7c).

The frequent collateral deletion of *RNASEH2B* prompted us to test whether *RNASEH2B* loss in cancer cells could be an actionable vulnerability to PARP inhibition. To do so, we performed *ex-vivo* analysis on primary CLL cells derived from 21 of the 100 patient samples assayed above. Patient characteristics of selected samples were similar across groups (ED Table 1). RNase H2 status was confirmed by enzymatic assay of CLL lysates (Fig 4b) and short-term CLL cultures were established from peripheral blood leukocyte samples by stimulating their proliferation with IL21 and co-culture with CD40-ligand expressing MEFs (ED Fig 8a,b and Supplementary Fig. 2). *RNASEH2B*-deficient cells were found to be significantly more sensitive to PARPi and especially to talazoparib, with the degree of sensitivity correlating with number of *RNASEH2B* alleles lost (Fig 4c and ED Fig 8c).

We then asked whether RNase H2 deficiency also confers PARPi sensitivity to tumours in xenograft experiments, utilizing isogenic HCT116 cells with and without *RNASEH2A* deletion (ED Fig 2a,g,l). Cells were implanted in the flanks of CD1 nude mice and, following establishment of tumours, mice were treated with talazoparib given its higher trapping activity. While talazoparib treatment did not lead to tumor regression, we observed significantly higher sensitivity to talazoparib in tumours lacking RNase H2 (Fig 4d). Furthermore, a second xenograft experiment confirmed this sensitivity to be specific to RNase H2 loss as complementation with an *RNASEH2A* transgene abrogated PARPi sensitivity (ED Fig 8d). Taken together, we conclude that collateral loss of RNase H2 enhances the vulnerability of cancer cells to PARP-trapping drugs.

Finally, we note that genome-embedded ribonucleotides are by far the most abundant aberrant nucleotides in the genome of cycling cells13 and may thus represent a major source of the traps that mediate the cytotoxicity of PARPi alongside base excision repair (BER) intermediates. In support of this possibility, *RNASEH2A-KO* cells are more sensitive to PARPi than isogenic cell lines with homozygous mutations in the catalytic domain of DNA polymerase β (*POLB 188-190*), a key BER enzyme (ED Fig 9). We therefore propose a model whereby the RER pathway and TOP1 compete for the processing of genome-embedded ribonucleotides (Fig 4e). Whereas RNase H2 cleavage initiates their problem-free removal, the action of TOP1 on ribonucleotides create PARP-trapping DNA lesions that impair successful completion of DNA replication and the resulting burden of genomic lesions ultimately causes cell death. We propose that the manipulation of genomic ribonucleotide processing could be harnessed for therapeutic purposes and this strategy may expand the use of PARP inhibitors to some HR-proficient tumors.

Methods

Cell culture

HeLa, RPE1-hTERT and 293T cells were purchased from ATCC and grown in Dulbecco's Modified Eagle Medium (DMEM; Gibco/Thermo Fisher) supplemented with 10% fetal bovine serum (FBS; Wisent), 200 mM GlutaMAX, 1x non-essential amino acids (both Gibco/Thermo Fisher), 100U/ml penicillin and 100μg/ml streptomycin (Pen/Strep; Wisent). HCT116 *TP53-KO* cells34, a kind gift from B. Vogelstein (Johns Hopkins University School of Medicine), were maintained in modified McCoy's 5A medium (Gibco/Thermo Fisher) supplemented with 10% FBS and Pen/Strep. SUM149PT cells were purchased from Asterand BioScience and grown in a DMEM:F12 medium mixture (Gibco/Thermo Fisher) supplemented with 5% FBS, Pen/Strep, 1 μg/ml hydrocortisone and 5 μg/ml insulin (both Sigma). DLD-1 WT and *BRCA2-KO* cells were purchased from Horizon and maintained in RPMI media (Gibco/Thermo Fisher) supplemented with 10% FBS and Pen/Strep. All cell lines were grown at 37°C and 5% CO_2. HeLa, RPE1-hTERT (with the exception of *BRCA1-KO* and *POLB 188-190* clones) and HCT116 cells were grown at atmospheric O_2. RPE1-hTERT *BRCA1-KO* and *POLB 188-190* clones, as well as DLD-1 and SUM149PT cell lines were maintained at 3% O_2.

Lentiviral and retroviral transduction

To produce lentivirus, 4.5×10^6 293T cells in a 10-cm dish were transfected with packaging plasmids (5 μg pVSVg, 3 μg pMDLg/pRRE and 2.5 μg pRSV-Rev) along with 10 μg of transfer plasmid using calcium phosphate. Medium was refreshed 12-16 h later. Virus-containing supernatant was collected ~36-40 h post transfection, cleared through a 0.4 μm filter, supplemented with 4 μg/ml polybrene (Sigma) and used for infection of target cells. The TKOv1 library virus was prepared as previously described30. The following antibiotics were used for selection of transductants: puromycin (HeLa, SUM149PT: 2 μg/ml; RPE1-hTERT 15-20 μg/ml; each for 48-72 h unless indicated otherwise) and blasticidin (5 μg/ml, 4-5 d for all cell lines). Cells stably expressing FLAG-Cas9-2A-Blast were maintained in the presence of 2 μg/ml blasticidin.

To complement the HCT116 *TP53-KO RNASEH2A-KO* cell line, cells were infected with retroviral supernatant produced in amphotropic Phoenix packaging cells35 using either pMSCVpuro empty vector (EV) or pMSCVpuro-RNASEH2A-WT in the presence of 4 μg/ml polybrene (Sigma) and 48 h later selected for stable integration using 2 μg/ml puromycin.

RNASEH2A expression plasmids

A FLAG-tagged human RNASEH2A cDNA (NM_006397.2; encoding amino acids 2-299) and the D34A/D169A mutant31 were cloned into the pCW57.1 vector (a gift from David Root; Addgene #41393) using the Gateway system (Life Technologies/Thermo Fisher) according to the manufacturer's protocol. The P40D/Y210A mutations were generated by site-directed mutagenesis using the following primers (5'-3'): P40D – GGCCCAGCACGTCGCCCCTGCCCG (Forward - F), CGGGCAGGGGCGACGTGCTGGGCC (Reverse - R); Y210A – GTCTTGGGATCATTGGGGGCGCCTGAGCCATAATCAGT (F), ACTGATTATGGCTCAGGCGCCCCCAATGATCCCAAGA (R). Expression constructs were introduced into HeLa *RNASEH2A-KO* cells by lentiviral transduction and expression was induced by the addition of 1 μg/ml doxycycline (Clontech) 24 h prior to starting experiments. The pMSCVpuro-RNASEH2A-WT plasmid was generated by cloning the coding sequence of human RNASEH2A into pMSCVpuro-Dest, a Gateway-compatible version of pMSCVpuro (Clontech), and introduced into HCT116 *TP53-KO RNASEH2A-KO* cells by retroviral transduction.

sgRNA target sequences

sgRNAs targeting the following sequences (5' to 3') were used to generate CRISPR knockouts. *RNASEH2A:* TGCCCGCCTCATCGACGCCC and CCCGTGCTGGGTGCGCCCCT (for Hela *RNASEH2A-KO*), GACCCTATTGGAGAGCGAGC (for HeLa Cas9, RPE1-hTERT, HeLa DR-GFP); *RNASEH2B:* TCCACCACAACTTGATCAAG; *PARP1:* TAACGATGTCCACCAGGCCA; *BRCA1:* AAGGGTAGCTGTTAGAAGGC; *POLB:* GAGAACATCCATGTCACCAC; *LacZ:* CCCGAATCTCTATCGTGCGG; *PSMD1-1:* TGTGCGCTACGGAGCTGCAA; *PSMD1-2:* ACCAGAGCCACAATAAGCCA

PSMB2-1: ATGTTCTTGTCGCCTCCGAC; *PSMB2-2:* AATATTGTCCAGATGAAGGA; *EIF3D-1:* TGTAGGTTGCCTCCATGGCC; *EIF3D-2:* AGACGACCCTGTCATCCGCA; *TP53:* CAGAATGCAAGAAGCCCAGA.

Vectors expressing the Cas9n D10A nickase together with guide RNAs designed against exon 1 and intron 1 of human *RNASEH2A* were generated by cloning annealed DNA oligonucleotides into pSpCas9n(BB)-2A-GFP and pSpCas9n(BB)-2A-Puro vectors (Addgene plasmid #48140 and #48141, respectively; gifts from Feng Zhang) as previously described36. All other sgRNA-expressing constructs were generated by cloning annealed DNA oligonucleotides into lentiGuide-Puro or lentiCRISPR v2 vectors (Addgene #52963 and 52961, gifts from Feng Zhang) as previously described37.

RNA interference

TOP1 was targeted with 40 nM of either a custom siRNA (siTOP1, target site sequence AAGGACTCCATCAGATACTAT, Sigma) previously described[38] or an ON-TARGETplus SMARTpool siRNA (siTOP1-SP, L-005278-00, Dharmacon/BD Technologies), previously used to knock down TOP1[39–41]. A custom siRNA targeting Luciferase (siCTRL, CTTACGCTGAGTACTTCGA, Sigma) or an ON-TARGETplus non-targeting pool (siCTRL-SP, D-001810-10-05, Dharmacon/BD Technologies) were used as controls[42]. siRNA oligos were transfected in Opti-MEM reduced serum medium using Oligofectamine (Life Technologies/Thermo Fisher). To improve knockdown efficiency for the ON-TARGETplus siRNA, a second round of transfection was conducted after 24 h. Following siRNA transfection, cells were seeded either for cell cycle analysis (24 h post last transfection) or for immunofluorescence analysis (48 h post transfection) as described below. Knockdown was optimised to minimize cell death, while maintaining efficient TOP1 depletion (apoptosis levels   14% of control transfected cells).

DNA damaging drugs

PARP inhibitors olaparib, talazoparib and veliparib were purchased from Selleck Chemicals. Talazoparib for the xenograft experiments was a kind gift of T. Heffernan and N. Feng (The University of Texas MD Anderson Cancer Center). Methyl methanesulfonate (MMS) and aphidicolin were obtained from Sigma. Concentrations and durations of treatment are indicated in the sections below and in the respective figures.

Generation of Cas9-expressing cells

Cells were transduced with the Lenti-FLAG-Cas9-2A-Blast vector[30] and transductants were selected with blasticidin. Cells were then seeded at low densities (500-1,000 cells, depending on cell line) on 15-cm dishes and single colonies were isolated using glass cylinders. Cas9 expression was confirmed by immunoblotting and gene editing efficiency was tested as follows:

Cells were transduced at a low (~0.3) multiplicity of infection (MOI) with either a control *LacZ* sgRNA construct or sgRNA constructs targeting essential genes *PSMD1*, *PSMB2* and *EIF3D*[30] followed by puromycin selection. 2.5×10^4 cells were subsequently seeded in 6-well plates, medium was exchanged 3 days later and the experiment was terminated at day 6. Cells were trypsinized, resuspended in media and the live cell count was determined by trypan blue exclusion on a ViCELL instrument (Beckman Coulter). Cell numbers were plotted relative to sg*LacZ*-transduced samples.

Generation of CRISPR knockout cell lines

To establish HeLa and HCT116 *TP53-KO RNASEH2A-KO* cell lines, 0.5×10^6 cells were seeded in 6-well plates and transfected with two vectors encoding both Cas9n and sgRNAs targeting *RNASEH2A* (derivatives of pSpCas9n(BB)-2A-GFP and pSpCas9n(BB)-2A-Puro) using Lipofectamine 2000 (Life Technologies/Thermo Fisher). 48 h after transfection, single GFP-positive cells were sorted into 96-well plates on a BD FACSJazz instrument (BD Biosciences) and grown until colonies formed. *RNASEH2A-KO* clones were selected on the basis of the size of PCR amplicons from the targeted region to detect clones that underwent

editing, which was subsequently confirmed by Sanger sequencing. Oligonucleotides (5' to 3') used for PCR amplification and sequencing of targeted *RNASEH2A* loci were as follows: ACCCGCTCCTGCAGTATTAG and TCCCTTGGTGCAGTGCAATC. The absence of functional RNASEH2A was confirmed by immunoblotting, an RNase H2 activity assay and alkaline gel electrophoresis as described below. Functionally wild-type *RNASEH2A* clones were identified in parallel and used as controls.

To generate the remaining CRISPR-edited HeLa and RPE1-hTERT cell lines, cells were electroporated with 5 μg of vectors encoding either the sgRNA (lentiGuide-Puro, for cells stably expressing Cas9) or encoding both the sgRNA and Cas9 (lentiCRISPR v2) using an Amaxa Nucleofector II instrument (Lonza). 0.7×10^6 RPE1-hTERT cells in a buffer containing 100 mM Na_2HPO_4 (pH 7.75), 10 mM KCl and 11 mM $MgCl_2$ were electroporated using program T-23. For HeLa cells, the Amaxa Cell Line Nucleofector Kit R (Lonza) was used with program I-13 according to the manufacturer's instructions. Cells were re-plated into antibiotic-free McCoy's 5A media supplemented with 10% FBS and allowed to recover for 24 h. Puromycin was subsequently added to growth media to enrich for transfectants and removed 24 h later. Cells were then cultured for additional 3-5 days to provide time for gene editing and eventually seeded at low densities (400-1,000 cells, depending on cell line) on 15-cm dishes. Single colonies were isolated using glass cylinders two to three weeks later. SUM149PT Cas9 *RNASEH2B-KO* cells were generated by transient transfection of parental SUM149PT Cas9 cells with a lentiGuide-puro-sgRNASEH2B construct using Lipofectamine 2000 (Thermo Fisher) as per the manufacturers protocol (2 μg plasmid DNA and 2 μl of Lipofectamine 2000 was used for 1×10^5 cells in a 6-well plate). Transfected cells were selected with puromycin for 24 h, grown for additional 4 days and single clones were isolated as above.

Targeted clones were identified by immunofluorescence and/or immunoblotting and successful gene editing was confirmed by PCR and TIDE analysis (https://tide-calculator.nki.nl)[43]. The following PCR primers (5' to 3') were used for amplification of targeted loci in *RNASEH2A*: AGATCTGGAGGCGCTGAAAGTGG (F), AGTGGCTGTATCATGTGACAGGG (R); *RNASEH2B:* TAGATGGTGTGCTGTGTGG (F), TGCTCAGCTTGTCATTGACC (R); *BRCA1:* TCTCAAAGTATTTCATTTTCTTGGTGCC (F), TGAGCAAGGATCATAAAATGTTGG (R); *PARP1:* AAGCAAACAGGACTGCCAGC (F), TACGCCACTGCACTCCAGC (R); *POLB:* TTACTGTTGTCATCACAGATTCTGC (F), AGCAACTCATGGAAGAATAATAGG (R); *TP53:* GCATTGAAGTCTCATGGAAGC (F); TCACTGCCATGGAGGAGC (R).

Generation of HeLa FUCCI WT and *RNASEH2A* KO cells

To establish HeLa WT and *RNASEH2A-KO* cells expressing the FUCCI cell cycle reporters mKO2-Cdt1 and mAG-Geminin.[32] HeLa WT and *RNASEH2A-KO* cells were transduced at a low MOI with pLenti6-mKO2-Cdt1 and pLenti6-mAG-Geminin vectors and transductants were selected with 2 μg/ml blasticidin. Subsequently, cells positive for both mKO2-Cdt1 and mAG-Geminin fluorescence were collected by sorting on a BD Biosciences FACS Aria II

instrument, expanded and used for further experiments. Expression of mKO2-Cdt1 and mAG-Geminin was confirmed by immunofluorescence and FACS analysis.

CRISPR/Cas9 screening

CRISPR screens were performed as described[30]. Cas9-expressing cells were transduced with the lentiviral TKOv1 library at a low MOI (~0.2-0.3) and puromycin-containing media was added the next day to select for transductants. Selection was continued until 72 h post transduction, which was considered the initial time point, t0. At this point the transduced cells were split into technical triplicates. During negative-selection screens (for PARPi sensitizers), cells were subcultured at day 3 (t3) and at day 6 (t6) each of the three replicates was divided into two populations. One was left untreated and an to the other an LD20 dose of olaparib (HeLa: 2 μM, RPE1-hTERT: 0.5 μM, SUM149PT: 0.2 μM) was added. Cells were grown with or without olaparib until t15 and subcultured every three days. Sample cell pellets were frozen at each time point for genomic DNA (gDNA) isolation. A library coverage of 200 cells/sgRNA was maintained at every step. Positive-selection screens (for suppressors of sensitivity) were carried out in a similar way, but the untreated control was left out, an LD80 dose of talazoparib was used (20 and 50 nM for HeLa and RPE1-hTERT, respectively), cells were subcultured only once after drug addition (t12 – t13) and screens were terminated at t18. Library coverage was 100 cells / sgRNA.

gDNA from cell pellets was isolated using the QIAamp Blood Maxi Kit (Qiagen) and genome-integrated sgRNA sequences were amplified by PCR using the KAPA HiFi HotStart ReadyMix (Kapa Biosystems). i5 and i7 multiplexing barcodes were added in a second round of PCR and final gel-purified products were sequenced on Illumina HiSeq2500 or NextSeq500 systems to determine sgRNA representation in each sample. DrugZ (see *Related Manuscript File*) was used to identify gene knockouts, which were depleted from olaparib-treated t15 populations but not depleted from untreated cells. Gene knockouts enriched at t18 as compared to t6 in positive-selection screens were identified using MAGeCK[33].

Gene ontology and interaction network analyses

PANTHER (http://pantherdb.org)[44] was used to identify gene ontology (GO) biological processes enriched in datasets of screen hits as compared to genome-wide representation. Hits [false discovery rate (FDR) 0.01 in at least one cell line + FDR 0.1 in at least 2 cell lines] from individual cell lines or hits common to at least two cell lines were analyzed with the "statistical overrepresentation test" (GO ontology database released 2017-02-28; annotation data set 'GO biological process complete') with Bonferonni correction for multiple testing. Mapping of the hits on the HumanMine protein interaction network was done through the esyN interface (http://www.esyn.org/). The network was then exported and visualized in Cytoscape version 3.4.0 (http://www.cytoscape.org/) and the node sizes adjusted to be proportional to the averaged DrugZ score over the three cell lines.

Clonogenic survival assays

To determine PARPi sensitivity cells were seeded on 10-cm dishes (500-3,000 cells/plate, depending on cell line and genotype) into drug-free media or media containing a range of

PARPi concentrations. Cells were either treated either for 2 days with talazoparib followed by additional 9-12 days of growth in drug-free media (HeLa, SUM149PT), treated for 7 days with talazoparib followed by 5-6 days in drug-free media (RPE1-hTERT, HCT116), or treated continuously for 12-13 days with olaparib. The cultures were incubated at 3% O_2, with the exception of the experiment in Fig 3g, which was carried out at atmospheric O_2. Medium (with or without PARPi) was refreshed every 4-7 days in all cases. At the end of the experiment medium was removed, cells were rinsed with PBS and stained with 0.4% (w/v) crystal violet in 20% (v/v) methanol for 30 mins. The stain was aspirated and plates were rinsed 2x in ddH_2O and air-dried. Colonies were manually counted and data were plotted as surviving fractions relative to untreated cells. To calculate EC50 values the data were fit to a three-parameter dose response model ['log(inhibitor) vs. normalized response'] using the non-linear regression function in Graphpad PRISM v6.0.

To analyze the synthetic lethality of combined *BRCA1* and *RNASEH2B* knockouts, RPE1-hTERT Cas9 *TP53-KO* WT and *BRCA1-KO* cells were transduced at a high (>1.0) MOI with lentiGuide sgRNA constructs targeting either *RNASEH2B* or *LacZ* (control) and seeded for clonal growth 48 h later. WT and *BRCA1-KO* colonies were grown at 3% O_2 for 12 and 20 days (due to slower growth of BRCA1-deficient cells), respectively. Synthetic lethality between RNase H2 and BRCA2 was assessed by transducing DLD-1 WT and *BRCA2-KO* cells with either an empty lentiCRISPR v2 vector or lentiCRISPR v2 constructs carrying sg*RNASEH2A* or sg*RNASEH2B*. Cells were selected with puromycin and seeded for clonogenic assays 7 days post infection. Clones were grown at 3% O2 for 11 (WT) or 14 days (*BRCA2-KO*).

Immunofluorescence microscopy

To analyze γ-H2AX focus formation, cells were grown on coverslips for 24 h, incubated in media containing 10 μM EdU for 20 min to label cells undergoing DNA replication, then pre-extracted for 5 min on ice with ice-cold buffer (25 mM HEPES, pH 7.4, 50 mM NaCl, 1 mM EDTA, 3 mM $MgCl_2$, 300 mM sucrose and 0.5% Triton X-100) and fixed with 4% paraformaldehyde (PFA) for 15 min at room temperature (RT). After fixation, cells were washed with PBS and blocked in 3% fetal cals serum (FCS) in PBS for 30 min at RT. EdU immunolabeling was performed using the Click-iT EdU Imaging Kit (Invitrogen, C10337). Afterwards cells were incubated with a primary mouse antibody against γ-H2AX (Millipore 05-636; 1:800) for 1.5 h at RT and then stained with anti-mouse secondary antibodies conjugated to Alexa Fluor-568 (Life Technologies) for 1 h at RT. Coverslips were mounted using Vectashield antifade mounting medium with 4,6-diamidino-2-phenylindole (DAPI; Vector Laboratories). For quantification of γ-H2AX foci images were visualized on a Zeiss Axioplan 2 microscope with a 40× Plan-neofluar objective, captured using Micro-Manager (http://open-imaging.com/) and analyzed using an ImageJ-based script as previously described[45]. Nuclei were defined on the basis of DAPI staining, and γ-H2AX foci were detected using the "Find maxima" function of ImageJ within each nuclear region. Exposure time, binning, microscope settings, light source intensity and the noise level in the "Find maxima" function were kept constant for all the samples within each individual experiment. More than 100 cells were analyzed per condition in each experiment.

For combined γ-H2AX / RAD51 immunofluorescence, 0.25×10^6 cells were seeded on coverslips and ~24 h later were subjected to 3 Gy X-irradiation. 2, 4 or 6 h post irradiation cells were incubated with nuclear extraction buffer (20 mM HEPES pH 7.4, 20 mM NaCl, 5 mM $MgCl_2$, 0.5% NP-40, 1 mM DTT and protease inhibitors) for 10 min on ice, rinsed with ice-cold PBS and subsequently fixed with 4% PFA for 10 min at RT. Cells were blocked in IF blocking buffer (10% goat serum, 0.5% NP-40, 0.5% saponin in PBS) for 30 min and incubated with primary antibodies diluted in blocking buffer (Santa-Cruz Biotechnologies rabbit anti-RAD51 / Millipore mouse anti-γ-H2AX; 1:150 and 1:2,000, respectively) for 2 h at RT. Cells were then washed with PBS (3x 5 min) and stained with fluorescent secondary antibodies (Alexa Fluor 488-conjugated goat anti-rabbit IgG and Alexa Fluor 555-conjugated goat anti-mouse IgG, Life Technologies/Thermo Fisher; 1:1,000 in blocking buffer) and 0.5 µg/ml DAPI for 1 h at RT. Cells were washed as above, mounted in ProLong Gold mounting media (Life Technologies/Thermo Fisher) and imaged used a Zeiss LSM780 laser-scanning microscope. Cells with more than 5 colocalizing γ-H2AX and RAD51 foci were quantified by manual counting. At least 100 cells per condition were analyzed in each experiment.

Immunofluorescence/flow cytometry (IF/FACS)

For detection of apoptotic cells by cleaved caspase-3 IF/FACS, 0.5×10^6 cells were plated on 6-cm dishes and either left untreated or treated with PARPi for 48 h (PARPi doses are indicated in respective figures). For analysis of apoptotic cells following TOP1 depletion, 0.25×10^6 cells were plated on 6-cm dishes, transfected with siCTRL or siTOP1 the next day and 24 h post-transfection were either left untreated or treated with PARPi for 48 h. Medium was removed and stored in a conical tube, cells were harvested by trypsinization, resuspended in the original conditioned media and centrifuged at 1,500RPM for 5 min at 4°C. Pellets were washed in PBS and fixed in 1 ml 4% PFA for 10 min at RT. Cells were pelleted as above, resuspended in 100 µl PBS and chilled on ice. 900 µl of -20°C methanol was then added drop-wise while gently vortexing. Fixed cells were stored at -20°C overnight or longer.

Before staining, cells were spun down as above, washed in PBS and blocked in IF blocking buffer (see 'Immunofluorescence' above). Cells were then centrifuged and resuspended in 200 µl of diluted rabbit anti-cleaved caspase-3 antibody (Cell Signaling #9661; 1:800 in IF blocking buffer). After 2 h incubation the antibody was diluted with 2 ml PBS, cells were spun down, and incubated for 1 h in 200 µl Alexa Fluor 488-conjugated goat anti-rabbit secondary antibody (Molecular Probes/Thermo Fisher, 1:1,000 in IF blocking buffer). The antibody was diluted with 2 ml PBS, cells were centrifuged, resuspended in 1 ml PBS and cleaved caspase-3 signal was analyzed on a BD FACSCalibur or BD LSRFortessa X-20 instruments. Data were analyzed using FlowJo software (Tree Star). See Supplementary Figure 2 for examples of gating strategies.

For analysis of recovery from talazoparib-induced replication blockage, cells were treated with 1 µM talazoparib for 24 h, washed extensively with PBS and grown in drug-free media for additional 10, 24 or 34 h. Cells were then harvested, fixed, stained as described above

using an anti-γH2AX primary antibody (JBW301, Millipore #05-636, 1:1,000 in blocking buffer) and finally DNA was labeled with propidium iodide (see below).

Cell cycle analysis by FACS

0.5×10^6 cells were seeded on 6-cm dishes into media with or without PARPi (doses and durations are indicated in respective figures). Cells were then harvested by trypsinization, resuspended in media and centrifuged (1,000 RPM, 5 min, 4°C). Pellets were resuspended in PBS, centrifuged again and resuspended in 1 ml propidium iodide (PI) staining buffer (20 μg/ml PI, 0.02% Triton X-100, 0.2 mg/ml RNase A in PBS). Cells were stained for 15 min at 37°C and analyzed on a BD FACSCalibur or BD LSR Fortessa X-20 instruments.

For combined PI/EdU staining, cells were treated and harvested as above and fixed in 70% ethanol (added dropwise while gently vortexing) overnight at -20°C. Cells were then centrifuged as above, washed in PBS and incubated with 10μM Alexa Fluor 488 azide (Molecular Probes/Thermo Fisher) in a buffer containing 100 mM Tris-HCl pH 8.5, 1 mM $CuSO_4$ and 100 mM ascorbic acid for 30 min before centrifugation, washing in PBS and PI staining. See Supplementary Figure 2 for examples of gating strategies.

Sister chromatid exchange assay

0.5×10^6 HeLa cells were seeded in 10-cm dishes and BrdU (final concentration 10 μM) was added the next day. BrdU containing-medium was refreshed 24 h later and cells were grown for another 22 h (46 h BrdU incubation in total). 100 ng/ml KaryoMAX colcemid (Gibco/Thermo Fisher) was added for the final 2 h and cells were harvested as follows:

Growth medium was removed and stored in a conical tube. Cells were gently washed with 1 ml of trypsin (the trypsin wash was combined with the original media), trypsinized, resuspended in the original conditioned media (+trypsin wash) and centrifuged (1000 RPM, 5 min, 4°C). Cells were then washed with PBS, spun down, resuspended in pre-warmed 75 mM KCl and incubated for 30 min at 37°C. Cells were centrifuged again, the supernatant was removed and cells were fixed by drop-wise addition of 1 ml fixative (ice-cold methanol : acetic acid, 3:1) while gently vortexing. An additional 10 ml of fixative was then added and cells were fixed at 4°C for at least 16 h. Once fixed, metaphases were dropped on glass slides, rinsed with fixative and air-dried overnight (protected from light).

To visualize sister chromatid exchanges (SCE) slides were rehydrated in PBS for 5 min and stained with 2 μg/ml Hoechst 33342 (Molecular Probes/Thermo Fisher) in 2xSSC (final 300 mM NaCl, 30 mM sodium citrate, pH 7.0) for 15 min. Stained slides were placed in a plastic tray, covered with a thin layer of 2xSSC and irradiated with 254 nM UV light (~5400 J/m^2). Slides were subsequently dehydrated in a 70%, 95% and 100% ethanol series (5 min each), air-dried and mounted in DAPI-containing ProLong Gold mounting medium (Molecular Probes/Thermo Fisher). Images were captured on a Zeiss LSM780 laser-scanning microscope.

DR-GFP assay and quantitative image-based cytometry (QIBC)

HeLa DR-GFP cells (a gift from R. Greenberg) were transduced with either a lentiCRISPR v2 empty vector or sgRNA-expressing constructs targeting *RNASEH2A* or *RNASEH2B*. 7 days after transductions 4-5 x 10^3 cells were plated per well of 96-well imaging plates (Corning 3603) and next day either mock transfected or transfected with either 100 ng of a plasmid expressing I-SceI or a GFP-expressing plasmid (to assess transfection-efficiency) using Lipofectamine 2000. Medium was exchanged 6-8 h later and at 48 h post-transfection cells were fixed in 4% paraformaldehyde. Immunofluorescence for RNASEH2A was performed as described above and plates were imaged on an InCell Analyzer 6000 automated microscope (GE Life Sciences) with a 20x objective. Image analysis was performed using Columbus (PerkinElmer). Nuclei were segmented and a sum of DAPI intensity, mean RNASEH2A intensity and mean GFP intensity was quantified for each nucleus. Cells showing a DNA content between 1N and 2N were selected based on DAPI intensity, RNASEH2A-positive and -negative populations were separated and percentages of GFP-positive cells were calculated. Only RNASEH2A+ cells were analyzed in vector-infected samples, whereas only RNASEH2A- cells were considered in sgRNA-transduced samples. Percentages of GFP+ cells in each sample were normalized to the transfection efficiency of a control GFP plasmid.

Immunoblotting

Cell pellets were resuspended in hot 2x sample buffer (166.7 mM Tris-HCl pH 6.8, 2% SDS, 20 mM DTT, 10% glycerol, 0.01% bromophenol blue) at a concentration of 5 x 10^6 cells/ml and denatured at 95°C for 5 min. An equivalent of 0.25-1 x 10^5 cells was separated by SDS-PAGE and transferred to a nitrocellulose or PVDF (for RNASEH2B) membrane. Membranes were blocked with 5% milk / TBST (TBS + 0.1% Tween-20) for at least 1 h at RT and incubated with primary antibodies diluted in 5% milk/TBST overnight at 4°C. Membranes were then washed 3 times with TBST, incubated with horseradish peroxidase-conjugated secondary antibodies for 1 h at RT, washed again and protein bands were detected using the SuperSignal West Pico enhanced chemiluminescence reagent (Thermo Fisher).

To assess the efficiency of TOP1 depletion, whole cell extracts were obtained by lysis and sonication of cells in UTB buffer (8 M urea, 50 mM Tris-HCl, pH 7.5, 150 mM β-mercaptoethanol, protease inhibitor cocktail (Roche)). Whole cell extracts for RNase H activity assays and for determining protein levels of the RNase H2 subunits were prepared by lysing cells in 50 mM Tris-HCl pH 8.0, 280 mM NaCl, 0.5% NP-40, 0.2 mM EDTA, 0.2 mM EGTA, 10% glycerol (vol/vol), 1 mM DTT and 1 mM PMSF for 10 min on ice, and subsequent addition of an equal volume of 20 mM HEPES pH 7.9, 10 mM KCl, 1 mM EDTA, 10% glycerol (vol/vol), 1 mM DTT and 1 mM PMSF for an additional 10 min. Whole cell extracts were cleared by centrifugation (17,000 g for 10 min at 4°C) and protein concentration was determined by Bradford assay (Protein Assay Kit, BioRad). Protein samples (35 μg total protein) were run on NuPAGE 4–12% Bis-Tris Protein Gels (Thermo Fisher Scientific) and transferred to nitrocellulose or PVDF membranes. Membranes were blocked in 5% milk / TBST (TBS + 0.2% Tween-20) and immunoblotting was performed as described above.

Immunoprecipitation

Cells were collected by trypsinization, washed once with PBS supplemented with 1 μM ADP-HPD (PARG inhibitor; Enzo) and 4 x 10^6 cells were snap-frozen in liquid nitrogen and then lysed in 1 ml of lysis buffer [50 mM HEPES pH 8.0, 100 mM KCl, 2 mM EDTA, 0.5% NP-40, 10% glycerol, 1 mM DTT, complete protease inhibitor cocktail (Roche), 1 μM ADP-HPD]. Lysates were incubated with gentle rotation at 4°C for 15 min and then centrifuged at 15,000x g for 10 min. 50 μl of total cell lysates were used as "input" and 950 μl were incubated with 5 μl of mouse anti-PARP1 antibody [Enzo (F1-23) ALX-804-211-R050] for 5 h at 4 °C. Protein G-agarose beads (60 μl slurry; Pierce) were added for an additional hour. Beads were collected by centrifugation, washed four times with lysis buffer and eluted by boiling in 60 μl 2x sample buffer. Samples were run on an 8% SDS-PAGE gel and immunoblotting was performed as described above (see 'Immunobloting').

To analyze PARP1 poly(ADP-ribosylation) in a specific phase of the cell cycle, HeLa FUCCI WT or *RNASEH2A-KO* were trypsinized, washed once with PBS, collected in tubes with PBS supplemented with 3% FCS and 1 μM ADP-HPD, and sorted based on mKO2-Cdt1 (G1 phase) and mAG-Geminin (S/G2/M phases) fluorescence on a BD Biosciences FACS Aria II instrument. See Supplementary Figure 2 for examples of gating strategies. 4 x 10^6 FACS-sorted cells were snap-frozen and lysed as described above. Equivalent amounts of proteins (~0.5-1 mg) were incubated with 25 μl of PARP1-Trap_A pre-equilibrated bead slurry (ChromoTek) for 2.5 h at 4 °C, washed four times with lysis buffer and eluted by boiling in 2x sample loading buffer (31.25 mM Tris pH 6.8, 25% glycerol, 1% SDS, 0.01% bromophenol blue, β-mercaptoethanol) prior to immunoblotting. Samples were run on a NuPAGE 4–12% Bis-Tris Protein Gel (Thermo Fisher Scientific) and immunoblotting was performed as described above.

Antibodies

The following antibodies were used for immunofluorescence (IF) and immunoblotting (IB) at indicated dilutions: sheep anti-pan-RNase H2 (raised against human recombinant RNase H2[13], IB 1:1,000, IP 5 μl / 1 ml lysate); rabbit anti-RNASEH2C (Proteintech 16518-1-AP; IB 1:1,000); rabbit anti-RNASEH2A (Origene TA306706, IB 1:1,000); mouse anti-RNASEH2A (Abcam ab92876; IF 1:500); mouse anti-RNASEH2A G-10 (Santa Cruz Biotechnologies sc-515475; WB 1:1000); mouse anti-γH2AX JBW301 (Millipore 05-636, IF 1:800 – 1:2,000); rabbit anti-RAD51 H-92 (Santa Cruz Biotechnologies sc-8349, IF 1:150); rabbit anti-BRCA1[46] (IB 1:1,000); mouse anti-Cas9 (Diagenode C15200203, IB 1:1,000); rabbit anti-PARP1 H-250 (Santa Cruz Biotechnologies sc-7150, IB 1:1,000); mouse anti-PAR 10H (Enzo ALX-804-220-R100, IB 1:1,000); rabbit anti-Topoisomerase I (Abcam ab109374; IB 1:5,000); rabbit anti-DYKDDDDK (Cell Signaling Technologies 2368, IB 1:1,000); rabbit anti-actin (Sigma A2066, IB 1:5,000); mouse anti-α–tubulin DM1A (Millipore CP06, IB 1:5,000); mouse anti-α–tubulin B512 (Sigma T6074, IB 1:5,000); rabbit anti-GAPDH (Sigma G9545, IB 1:20,000); mouse anti-vinculin (Sigma V9264, IB 1:1,000); rabbit anti-DNA polymerase beta (Abcam ab26343, IB 1:1,000); rabbit anti-cleaved caspase-3 (Cell Signaling Technologies 9661S, IF 1:800).

Cell Titer Glo assay

200 cells per condition were plated on 96-well assay plates in technical triplicates either in drug-free media or in a range of MMS concentrations. MMS was washed out 24 h later and cells were grown in drug-free media for another 48 h. Cell viability was analyzed using the Cell Titer Glo assay kit (Promega) according to the manufacturer's instructions. Luminescence was read on an Envision 2104 plate reader (Perkin Elmer).

Detection of ribonucleotides in genomic DNA

Total nucleic acids were isolated from 10^6 cells by lysis in ice-cold buffer (20 mM Tris-HCl pH 7.5, 75 mM NaCl, 50 mM EDTA) and subsequent incubation with 200 μg/ml proteinase K (Roche) for 10 min on ice followed by addition of sarkosyl (Sigma) to a final concentration of 1%. Nucleic acids were sequentially extracted with TE-equilibrated phenol, phenol:chloroform:isoamyl alcohol (25:24:1), and chloroform, and then precipitated with isopropanol. Nucleic acids were collected by centrifugation, washed with 75% ethanol, air-dried and dissolved in nuclease-free water.

For alkaline gel electrophoresis, 500 ng of total nucleic acids were incubated with 1 pmol of purified recombinant human RNase H231 and 0.25 μg of DNase-free RNase (Roche) for 30 min at 37°C in 100 μl reaction buffer (60 mM KCl, 50 mM Tris-HCl pH 8.0, 10 mM MgCl$_2$, 0.01% BSA, 0.01% Triton X-100). Nucleic acids were ethanol-precipitated, dissolved in nuclease-free water and separated on a 0.7% agarose gel in 50 mM NaOH, 1 mM EDTA. After electrophoresis, the gel was neutralised in 0.7 M Tris-HCl pH 8.0, 1.5 M NaCl and stained with SYBR Gold (Invitrogen). Imaging was performed on a FLA-5100 imaging system (Fujifilm), and densitometry plots generated using an AIDA Image Analyzer (Raytest).

RNase H2 activity assay

Recombinant RNase H2 was expressed in Rosetta-2 *Escherichia coli* cells using a polycistronic construct based on pGEX6P1 (pMAR22) and purified as previously described31. Site-directed mutagenesis to introduce the D34A/D169A or P40D/Y210A mutations was performed using the Quikchange method (Agilent). To measure enzyme activity, a range of RNase H2 concentrations (0.06 – 2 nM) was incubated with 2 μM substrate in 5 μl reactions (in a buffer containing 60 mM KCl, 50 mM Tris-HCl pH 8.0, 10 mM MgCl$_2$, 0.01% BSA and 0.01% Triton X-100) at 37°C for 30 min or 1 h. Substrate was formed by annealing a 3'-fluorescein-labelled oligonucleotide (GATCTGAGCCTGGGaGCT, DRD:DNA, or gaucugagccugggagcu, RNA:DNA; uppercase DNA, lowercase RNA) to a complementary 5' DABCYL-labelled DNA oligonucleotide (Eurogentec). Reactions were stopped by adding an equal volume of 96% formamide, 20 mM EDTA, and heating at 95°C. Products were resolved by denaturing PAGE (20%, 1x TBE), visualized on a FLA-5100 imaging system (Fujifilm) and quantified using ImageQuant TL (GE Healthcare).

To assess RNase H2 activity in whole cell extracts a FRET-based fluorescent substrate release assay was performed as previously described31. RNase H2 specific activity was determined against a DRD:DNA substrate (described above). Activity against a double-

stranded DNA substrate of the same sequence was measured and used to correct for non-RNase H2 activity against the DRD:DNA substrate. Reactions were performed in 100 μl of buffer with 250 nM substrate in 96-well flat-bottomed plates at 25°C. Whole cell lysates were prepared as described above, and the final protein concentration used per reaction was 100 ng/μl. Fluorescence was read for 100 ms using a VICTOR2 1420 multilabel counter (Perkin Elmer), with a 480-nm excitation filter and a 535-nm emission filter.

Ex-vivo CLL studies

Peripheral blood mononuclear cells were isolated from blood samples collected from patients with a new or existing diagnosis of CLL, irrespective of the stage of disease or time/type of treatment from two Birmingham hospitals (Heartlands and Queen Elizabeth). This study was approved by the South Birmingham Ethics Committee (REC number 10/H1206/58), performed according to institutional guidelines and written consent was obtained from all participants.

Primary chronic lymphocytic leukemia (CLL) cells (5 x10^4) and CD40L-expressing mouse embryonic fibroblasts (5 x10^3) were seeded in each well of a 96-well plate (Corning) in 100 μl of RPMI media supplemented with 10% FBS (Sigma-Aldrich, UK) and 25 ng/ml IL-21 (eBioscience)47. After 24 h, 200 μl more media was gently added and cells were incubated for another 48 h. The media was then aspirated, replaced with 200 μl of media containing talazoparib and cells were incubated for a further 72 h. The cytotoxic effect of PARPi was determined by propidium iodide exclusion as measured by flow cytometry with an Accuri C6 flow cytometer (Applied Biosystems). Only cells, which entered the cell cycle upon stimulation (as determined by forward- and side-scatter FACS profiles), were considered for analysis. Data was expressed as a surviving fraction relative to untreated cells, for gating strategies see Supplementary Fig 2.

Multiplex Ligation-dependent Probe Amplification (MLPA) assay

Genomic DNA was isolated from primary CLL cells using the Flexigene kit (Qiagen). To identify deletions in *RNASEH2B* gene the MLPA assay was performed on approximately 100 ng of genomic DNA (gDNA) per sample using the P388-A2 SALSA MLPA kit (MRC-Holland) according to the manufacturer's protocol. 2 μl of amplified products were separated by capillary electrophoresis on an ABI PRISM 3130xl Genetic Analyzer (Applied Biosystems) with a GeneScan 600 LIZ Size Standard (Thermo Fisher). Data were analyzed using GeneMaker software v2.4.0 (SoftGenetics). Data were normalized using gDNA from 4 control reference samples. Copy number changes represented as a MLPA ratio were detected by comparing normalized peak intensities between the reference and the CLL samples. The MPLA ratio thresholds (X) were set as follows: 0.75 ≤ X ≤ 1.25, diploid sample; 0.4 ≤ X < 0.75, monoallelic deletion; X < 0.4, biallelic deletion. Samples showing either a standard deviation (SD) of control probes above 0.15, or samples with large Q fragment peaks and with more than 4 control probes having MLPA ratios out of diploid range were excluded from the analysis.

Comparative Genomic Hybridization (CGH) array

Genotyping of CLL samples was accomplished using HumanCoreExome BeadChip arrays (Illumina Inc., San Diego, USA) by UCL Genomics (UCL Great Ormond Street Institute of Child Health, London) in accordance with the Infinium HTS Assay protocol (15045736_A, Illumina Inc, San Diego, USA). Genotypes were called by GenomeStudio software Genotyping Module v.3.1 (Illumina). A call rate of 98% was accepted as the primary quality control for each sample. Log R Ratio and B Allele Frequency values generated by the GenomeStudio software were used to assess allelic losses in chromosome 13q.

Analysis of copy number alterations (CNA) in the RB1-RNASEH2B region in castration-resistant prostate cancer (CRPC)

CRPC (n=226) whole exome sequencing data generated by the International Stand Up To Cancer/Prostate Cancer Foundation Prostate Cancer Dream Team were downloaded and re-analysed[29,48]. Paired-end sequencing reads were aligned to the human reference genome (GRCh37/hg19) using BWA (0.5.9), with default settings and re-aligned using stampy (1.0.2). ASCAT (version 2.3) was used to estimate CNA, tumour purity and ploidy.

Xenograft experiments

Female athymic CD-1 nude mice (5–7 weeks old, Charles River Laboratories) were used for *in vivo* xenograft studies and quarantined for at least 1 week before experiments. Exponentially growing HCT116 *TP53-KO RNASEH2A-WT* or *RNASEH2A-KO* cells were injected subcutaneously into the bilateral flanks of each animal ($2x10^6$ cells per flank). Tumours were measured by caliper every 3 – 4 days and tumour volume was determined by the formula (length $\times$ width^2)/2. When the tumour volumes reached approximately 100 mm^3 (10 days after injection), mice were randomized into treatment and control groups (8 animals per group, 32 animals in total; sample size was determined based on previous relevant studies). Talazoparib [BMN673, 0.333 mg/kg, pharmacological grade, a kind gift of T. Heffernan and N. Feng (The University of Texas MD Anderson Cancer Center)] or vehicle [10% N,N-Dimethylacetamide (ACROS Organics), 5% Solutol HS 15 (Sigma-Aldrich) in PBS (Gibco)] was administered once daily by oral gavage (0.1 ml per 10 g of body weight) for the indicated length of time, or until the tumour reached the maximum size (15 mm in any direction) or ulcerated, or a body conditioning score of 2 was reached, as determined by UK Home Office regulations. The data reported is the average tumor volume per mouse. Individual flanks that showed no evidence of tumour growth before initiation of treatment were excluded from subsequent measurements and analysis.

A subsequent experiment was performed by injecting exponentially growing HCT116 *TP53-KO RNASEH2A-KO* cells complemented either with an empty vector (EV) or a vector encoding RNASEH2A-WT ($2x10^6$ cells per flank). To increase the potential treatment window, mice were randomized into treatment and control groups (8 animals per group, 32 animals in total), and treatment started 3 days after injection when palpable tumours were formed. The treatment was administered as described above. Animals that showed no evidence of tumour growth on both flanks within the first 11 days of treatment were excluded from analysis.

The technician performing tumour measurements was blinded to the experimental design/ identity of cells injected. All animal studies were carried out under Project Licence PPL 70/8897 approved by the UK Home Office and by the University of Edinburgh Animal Welfare and Ethical Review Body.

Statistical analysis

Data were analyzed using a two-tailed Student's t-test and a two-way ANOVA under the assumption of normal distribution for biological parameters. No corrections for multiple testing were made. Test used are indicated in respective figure legends. The number of samples (*n*) in figure legends represents independent biological replicates, unless stated otherwise. No statistical methods were used to determine the sample size prior to starting experiments. Cell biology experiments were not randomized and the investigators were not blinded with regards to sample allocation and evaluation of the experimental outcome. For xenograft experiments blinding and randomisation were performed.

Extended Data
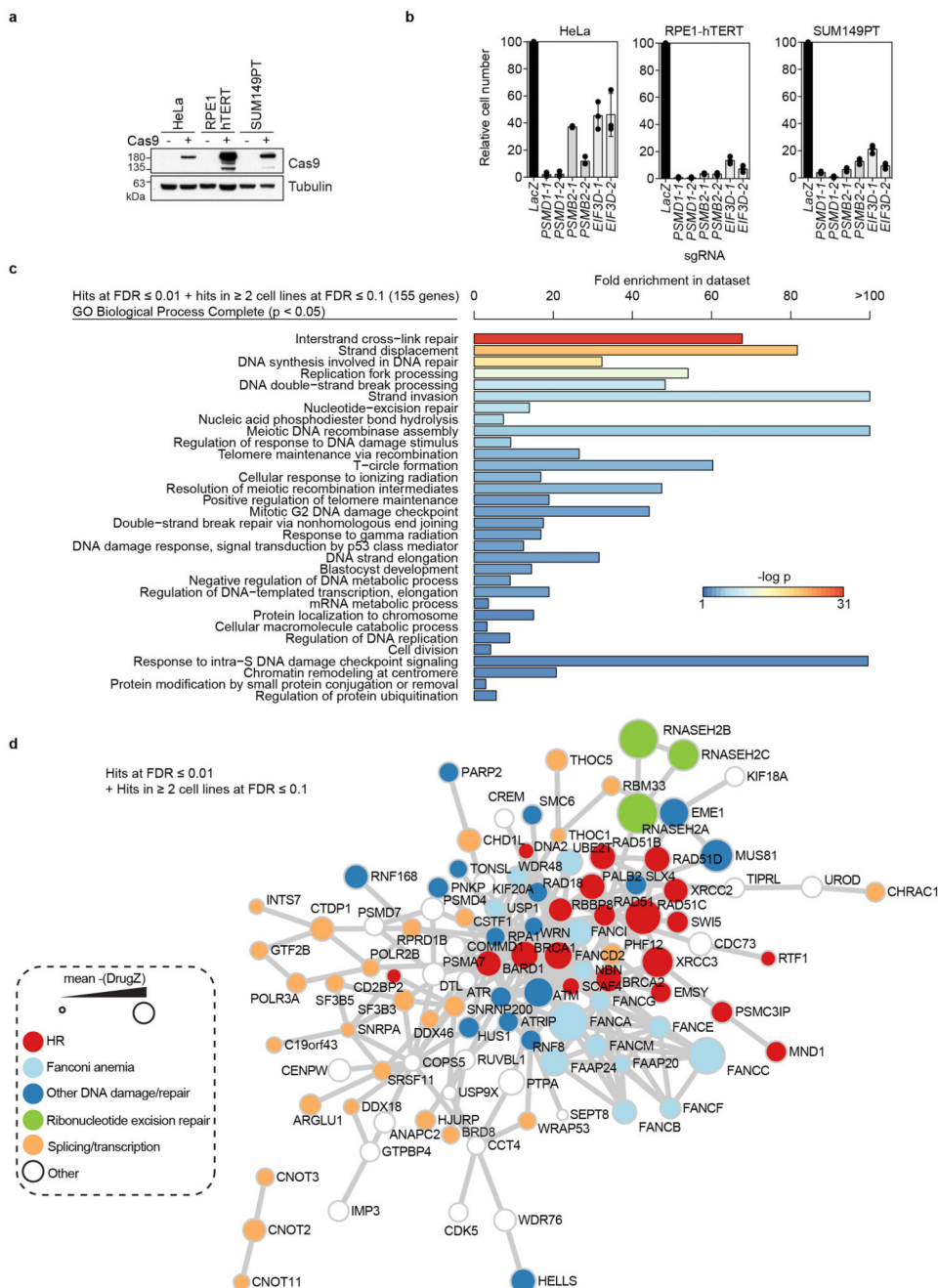
ED Figure 1.

Related to Figure 1. a, Cas9 immunoblot of whole cell extracts (WCEs) from parental HeLa, RPE1-hTERT and SUM149PT cells and clones stably transduced with a lentiviral FLAG-Cas9-2A-Blast construct (representative of $n \geq 2$ biologically independent experiments). Tubulin, loading control. **b,** Validation of CRISPR/Cas9 gene editing efficiency in Cas9-expressing HeLa, RPE1-hTERT and SUM149PT clones. Cell

proliferation was monitored after transduction with a control sgRNA construct (sg*LacZ*) or sgRNAs targeting essential genes *PSMD1*, *PSMB2* and *EIF3D*30. Solid circles, individual values. Bars, mean ±SD (normalized to sg*LacZ*, $n = 3$ technical replicates), **c,** Gene ontology (GO) terms significantly ($P < 0.05$, binomial test with Bonferroni correction) enriched among hits from olaparib screens common to at least two cell lines. Enrichment was analyzed using PANTHER. **d,** esyN network analysis of interactions between hits common to at least two cell lines. Node size corresponds to mean DrugZ score across cell lines. 77/155 genes are mapped on the network.
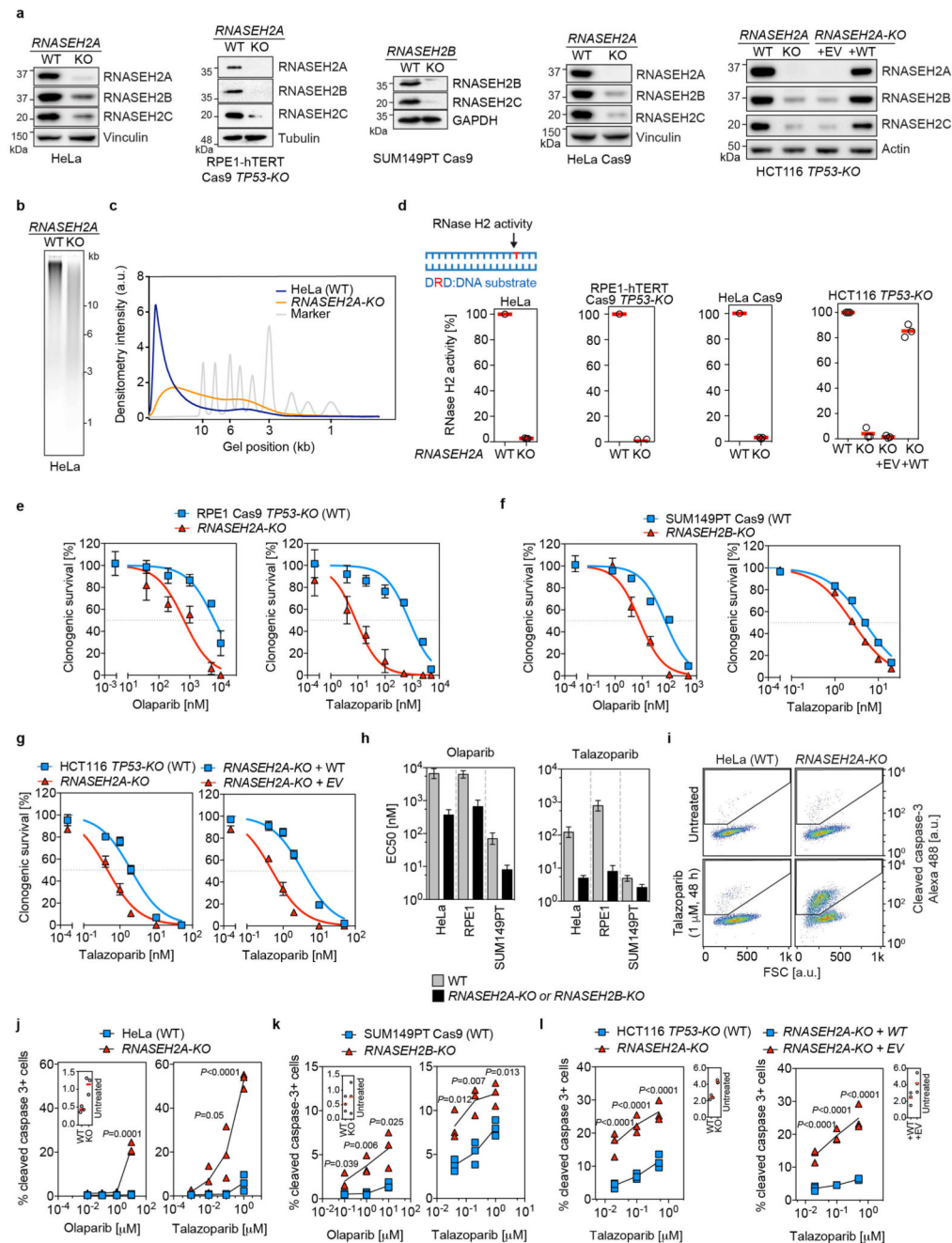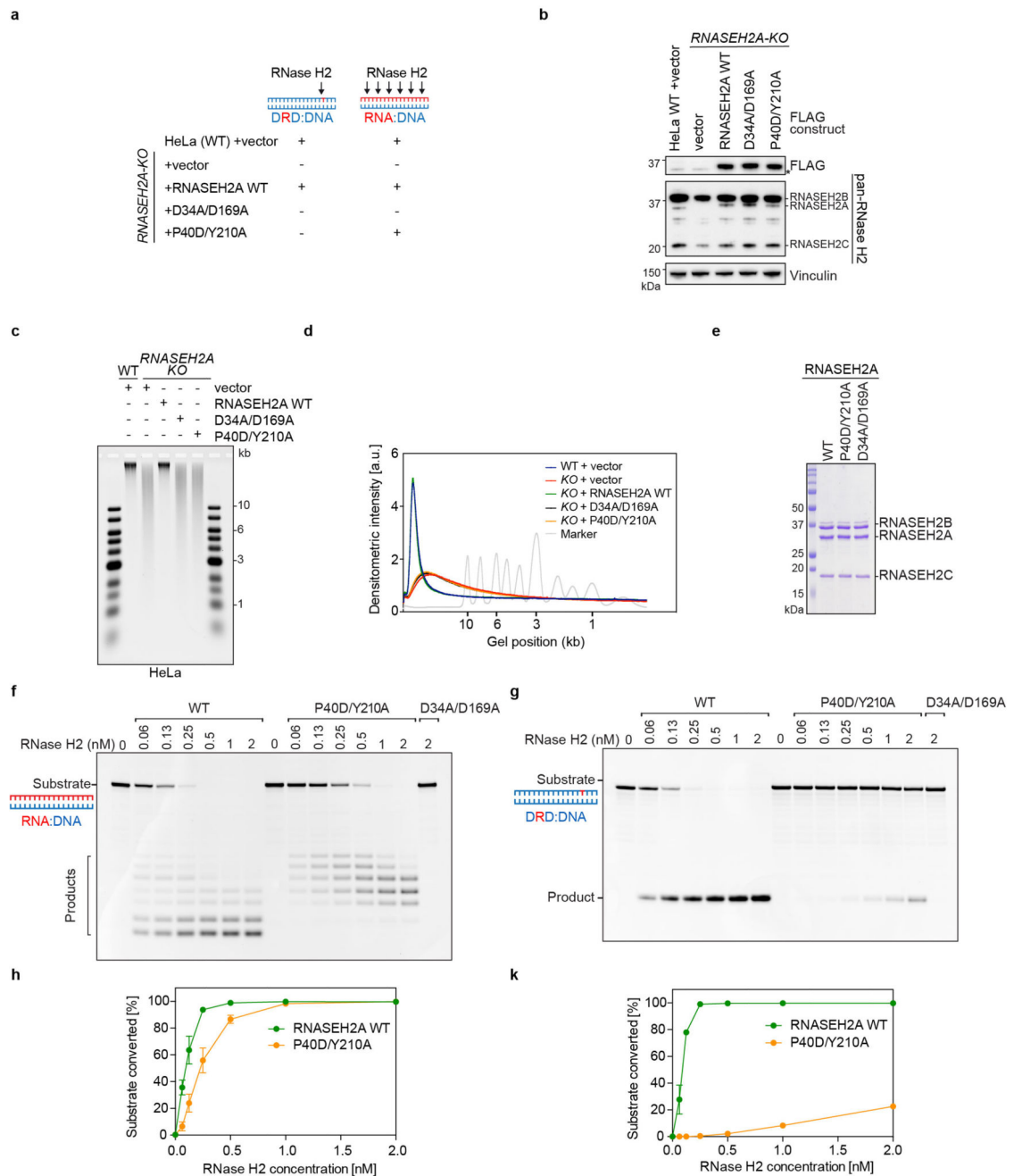
ED Figure 2.
Related to Figure 2a,b. a, CRISPR-mediated inactivation of *RNASEH2A* or *RNASEH2B* in the cell lines used in this manuscript. WCEs of indicated cell lines and genotypes were processed for immunoblotting using antibodies against RNASEH2A, RNASEH2B or RNASEH2C. Vinculin, tubulin and GAPDH, loading controls. Representative immunoblots (of *n* ≥ 2 biologically independent experiments). **b-d.** Abolished RNase H2 enzymatic activity and increased levels of genome-embedded ribonucleotides in *RNASEH2A-KO* cells. **b.** Representative (*n* = 3 biologically independent experiments) analysis of total nucleic

acids from WT and *RNASEH2A-KO* HeLa cells treated with recombinant RNase H2 and separated by alkaline agarose gel electrophoresis. Ribonucleotide-containing genomic DNA from *RNASEH2A-KO* HeLa cells is nicked and therefore has increased electrophoretic mobility13. **c,** Densitometric quantification of the alkaline gel shown in **b**. **d,** Cleavage of an RNase H2-specific double-stranded DNA oligonucleotide with a single incorporated ribonucleotide (DRD:DNA; ribonucleotide position is shown in red) by WT and *RNASEH2A-KO* WCEs of the indicated cell types was measured using a fluorescence quenching-based assay31. Individual values (open circles) with mean (red lines, $n = 3$ biologically independent experiments). **e-l,** RNase H2 deficiency leads to PARPi sensitivity in multiple cell types. **e-h,** Clonogenic survival assays of the indicated cell lines treated with the indicated PARPi. Mean ±SD, normalized to untreated cells ($n = 3$ biologically independent experiments). Solid lines, nonlinear least squares fit of the data to a three-parameter dose response model. **h.** EC50 values for olaparib (left) and talazoparib (right) in the indicated cell lines as determined by nonlinear least squares fitting of data in **e, f, g** and Fig 2a,b. Bars, EC50 value ± 95% confidence interval. **i-l,** Increased apoptosis in HeLa *RNASEH2A-KO,* SUM149PT Cas9 *RNASEH2B-KO* and HCT116 *RNASEH2A-KO* cells following PARPi treatment. **i**, Representative ($n = 3$ biologically independent experiments) cleaved caspase-3 immunofluorescence / flow cytometry (IF/FACS) profiles of untreated and talazoparib-treated HeLa WT and *RNASEH2A-KO* cells. FSC = forward scatter. **j-l,** Percentages of cleaved caspase-3-positive (caspase-3+) cells of the indicated genotypes treated with the indicated PARPi. Individual values (coloured symbols) with mean (solid lines, $n = 3$ biologically independent experiments). Inset: Levels of cleaved caspase-3+ cells without PARPi treatment. Red lines, mean ($n = 3$ biologically independent experiments). *P* values, unpaired two-tailed t-test. In **a**, **d**, **g** and **l**, HCT116 *RNASEH2A-KO* cells were transduced either with an empty vector (+EV) or a full-length RNASEH2A expression construct (+WT), where indicated.
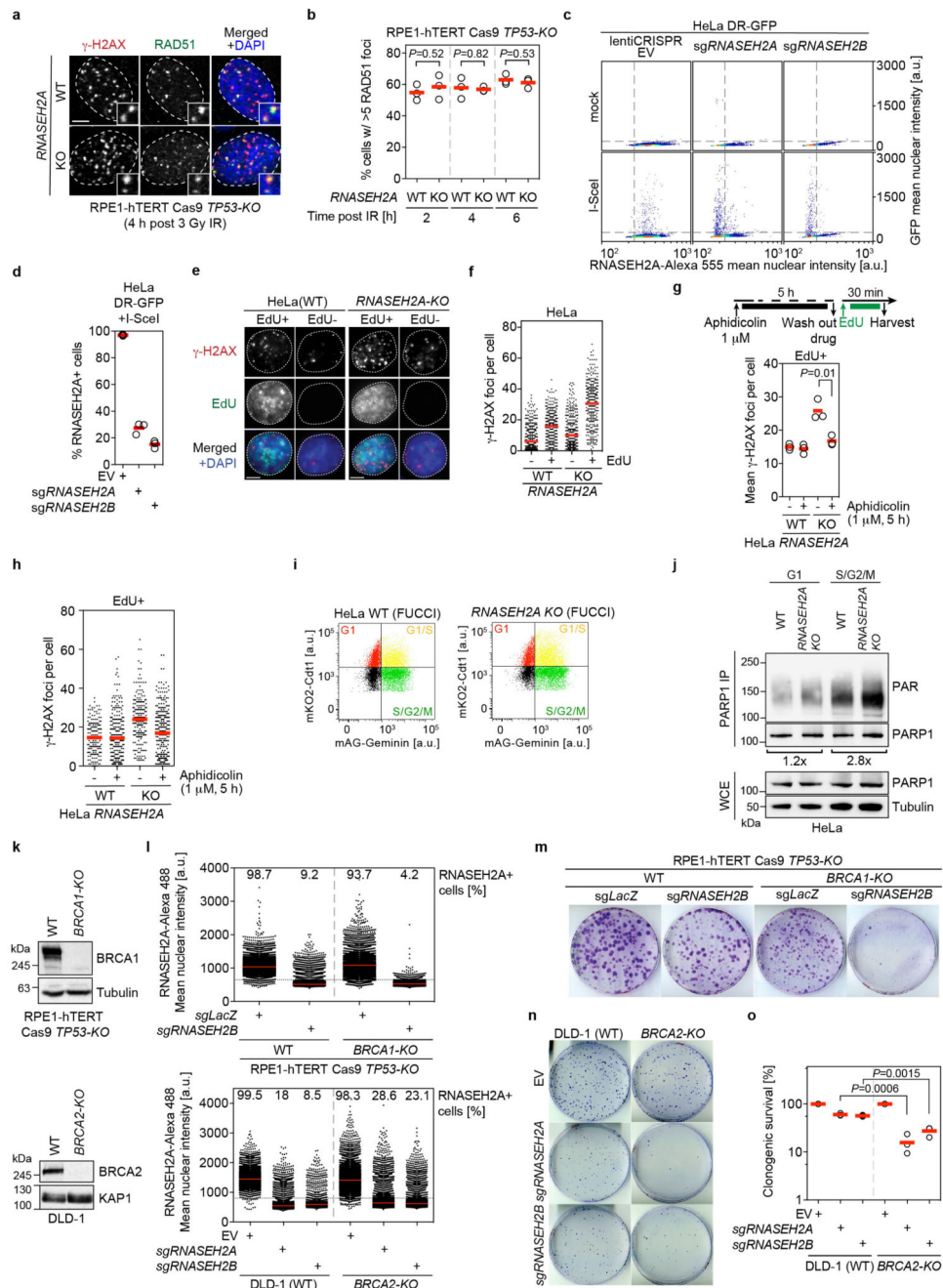
ED Figure 3.

Related to Figure 2. a-d, HR is not affected by inactivation of RNase H2. **a,** Representative micrographs (n = 3 biologically independent experiments) of RPE1-hTERT Cas9 *TP53-KO* (WT) and *RNASEH2A-KO* cells exposed to 3 Gy of X-rays (IR) and processed for γ-H2AX and RAD51 immunofluorescence (IF) 4 h later. **b.** Quantification of the experiment in **a** at the indicated time points after IR, plotted as percentage of cells with >5 γ-H2AX and RAD51 colocalizing foci. Individual values (open circles) with mean (red lines, n = 3 biologically independent experiments). *P* values, unpaired two-tailed t-test. **c,** Representative

(*n* = 3 biologically independent experiments) quantitative image-based cytometry (QIBC) plots of DR-GFP experiments in Fig 2e. Each point shows the mean GFP and RNASEH2A IF intensities per nucleus of mock- or I-SceI-transfected HeLa DR-GFP cells transduced with indicated Cas9/sgRNA constructs (EV = empty vector). Dashed lines separate RNASEH2A+/- and GFP+/- cell populations. **d,** Quantification of RNASEH2A+ cells in DR-GFP experiments shown in **c** and Fig 2e as determined by QIBC. Individual values (open circles) with mean (red lines; *n* = 3 biologically independent experiments). **e-h,** Replication-dependent endogenous DNA damage in RNase H2-deficient cells. **e,** Representative (*n* = 3 biologically independent experiments) micrographs for experiments quantified in Fig 2g. γ-H2AX immunofluorescence (IF) in EdU positive (EdU+) and negative (EdU-) WT and RNASEH2A-KO HeLa cells. Scale bars, 5 μm. **f,** Quantification of γ-H2AX foci per nucleus in experiments shown in **e** and Fig 2g. Dots, foci number in individual nuclei. Red lines, mean (*n* = 3 biologically independent experiments). **g,h**. HeLa WT and *RNASEH2A-KO* cells were treated with aphidicolin and EdU as indicated in the schematic (top), and immunostained with antibodies to γ-H2AX. Mean number of foci per EdU-positive (EdU+) nucleus in each experiment (**g**, open circles) or the number of foci in individual EdU+ nuclei (**h**, dots). Red lines, mean (*n* = 3 biologically independent experiments, 100 cells / sample / experiment analyzed). *P* value, unpaired two-tailed t-test. **i, j,** Increased poly(ADP-ribosylation) of PARP1 in G1 as well as in S/G2/M phases in *RNASEH2A-KO* cells. **i,** Representative (*n* = 2 biologically independent experiments) FACS plots of HeLa WT and *RNASEH2A KO* cells expressing the FUCCI cell cycle reporters mKO2-Cdt1 and mAG-Geminin32. **j,** PARP1 immunoprecipitates from WCEs of FUCCI-sorted G1 or S/G2/M HeLa WT and *RNASEH2A-KO* cells, probed with the indicated antibodies in immunoblotting (representative of *n* = 2 biologically independent experiments). Tubulin, loading control. Densitometric quantification of PAR signals normalized to immunoprecipitated PARP1 is shown as fold changes from WT to *RNASEH2A-KO* cells. **k-o,** Inactivation of RNase H2 in *BRCA1-* or *BRCA2*-deficient backgrounds results in synthetic lethality. **k,** BRCA1 and BRCA2 expression, respectively, in RPE1-hTERT *TP53-KO* WT and *BRCA1-KO* (top) or DLD-1 WT and *BRCA2-KO* (bottom) cells. WCEs were processed for immunoblotting with the indicated antibodies. Tubulin and KAP1, loading controls. Representative of *n* 2 biologically independent experiments. **l,** RNase H2 levels in cells used in m, **n, o** (bottom) and Fig 2i. Cells were transduced with the indicated sgRNA- (top) or Cas9/sgRNA vectors (bottom; EV = empty vector) and processed for RNASEH2A IF. Each point represents mean RNASEH2A intensity per nucleus as measured by QIBC (*n* = 1 experiment). 2000 cells analyzed per sample. Percentages of RNASEH2A+ cells in individual samples are shown above each plot. **m,** Representative images (*n* = 3 biologically independent experiments) of clonogenic survival assays quantified in Fig 2i. **n, o,** Synthetic lethality after inactivation of *RNASEH2A* or *RNASEH2B* in *BRCA2*-deficient cells. Clonogenic survival of DLD-1 WT and *BRCA2-KO* cells was assessed after transduction with indicated Cas9/sgRNA vectors. **n**, Representative images of *n* = 3 biologically independent experiments. **o,** Quantification of the experiment in **n**. Individual values (open circles) with mean (red lines; *n* = 3 biologically independent experiments). *P* values, unpaired two-tailed t-test.

ED Figure 4.

Related to Figure 2j. RNASEH2A P40D/Y210A is a separation-of-function mutant that cannot excise single DNA-embedded ribonucleotides, but cleaves RNA:DNA heteroduplexes (similar to the yeast *rnh201-P45D-Y219A* mutant16). **a,** Schematic depicting enzymatic activity against two different RNase H2 substrates (DRD:DNA, dsDNA with embedded ribonucleotide, or RNA:DNA hybrids) in cell lines used in **b-d** and Fig 2j. WT and *RNASEH2A-KO* cells were transduced with either an empty vector (EV) or the indicated RNASEH2A constructs. **b,** Complementation of HeLa *RNASEH2A-KO* cells with

FLAG-tagged RNASEH2A variants restores RNase H2 complex protein levels. WCEs from HeLa WT and *RNASEH2A-KO* cells stably expressing indicated lentiviral constructs were processed for immunoblotting with the indicated antibodies. Vinculin, loading control. Asterisk indicates a non-specific band. Representative of $n = 3$ biologically independent experiments. **c,d,** Complementation of HeLa *RNASEH2A-KO* cells with WT RNASEH2A, but not with the D34A/D169A (catalytic-dead) or P40D/Y210A (separation-of-function) mutants, rescues increased levels of genome-embedded ribonucleotides. **c,** Total nucleic acids from the cell lines shown in **a**, **b** were treated with recombinant RNase H2 and separated by alkaline agarose gel electrophoresis (representative of $n = 4$ experiments). **d,** Densitometric quantification of alkaline gel shown in **c**. **e,** Purified human RNase H2 complexes consisting of RNASEH2B, RNASEH2C and either RNASEH2A WT, P40D/ Y210A or D34A/D169A subunits separated by SDS-PAGE and stained with Coomassie Blue ($n = 1$). **f-k,** RNase H2 activity assays with fluorescein-labeled RNA:DNA substrate (**f**) or double-stranded DNA with a single incorporated ribonucleotide (DRD:DNA) (**g**) and increasing amounts of recombinant WT, P40D/Y210A or D34A/D169A RNase H2. Products were separated by polyacrylamide gel electrophoresis and detected by fluorescence imaging. Representative of $n = 3$ biologically independent experiments. **h,k,** Quantification of **f**, **g**. Product signal plotted relative to substrate signal per lane. Mean ±SD ($n = 3$ biologically independent experiments).
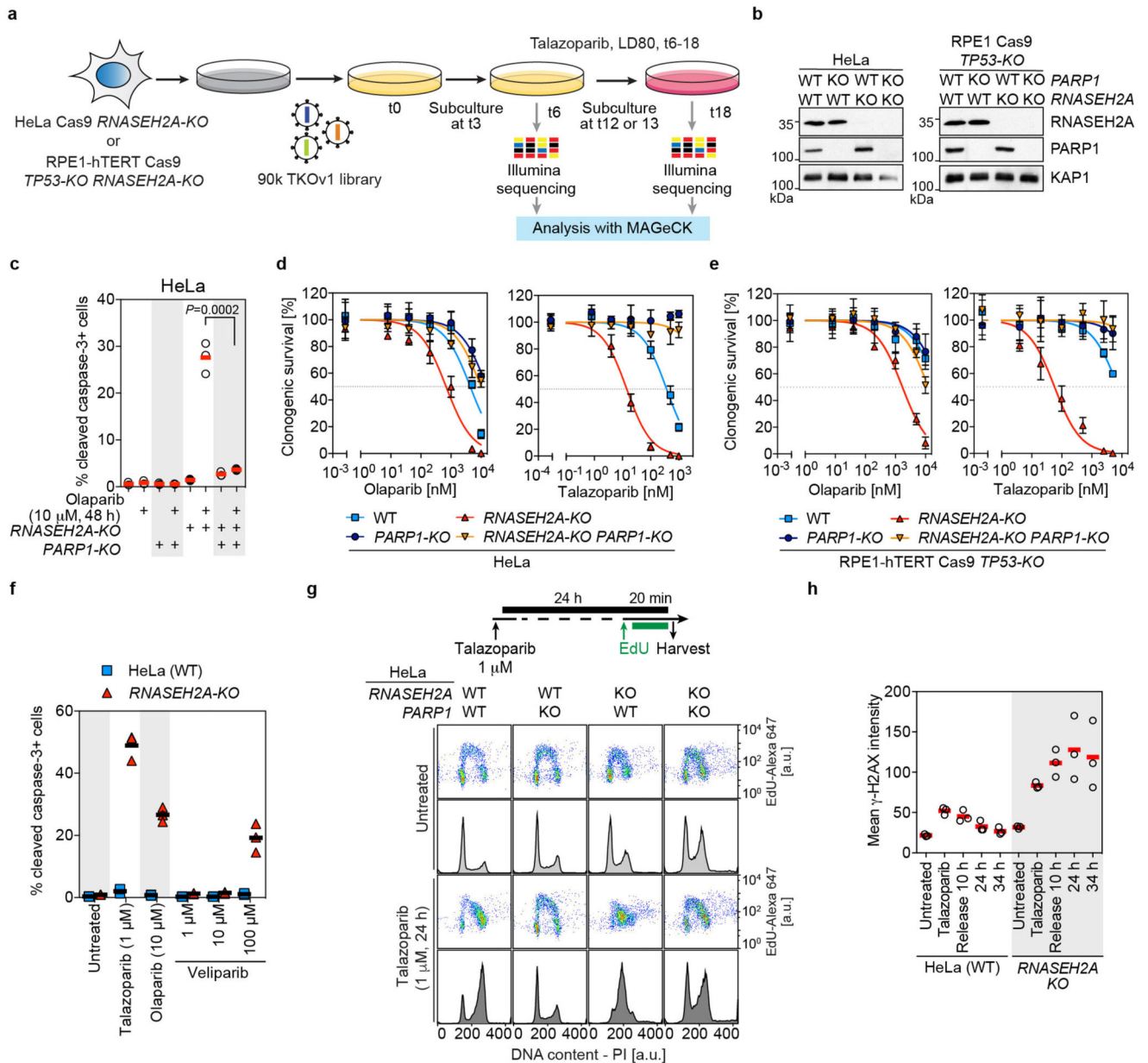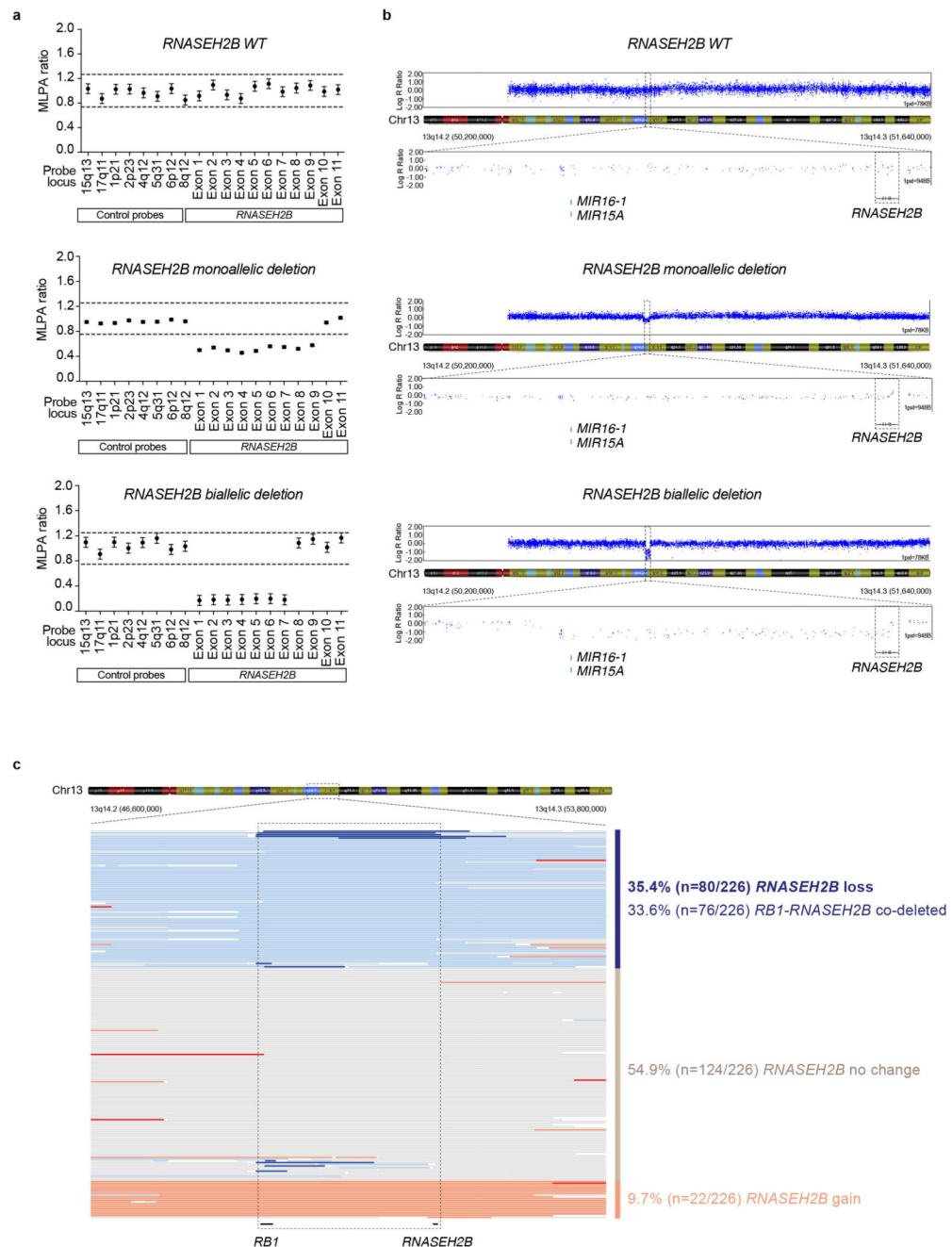
ED Figure 5.

Related to Fig 3a-c. PARP1 trapping is the underlying cause of PARPi sensitivity in RNase H2-deficient cells. a, Schematic representation of CRISPR screens for suppressors of talazoparib sensitivity in RNase H2-deficient cells. Cas9-expressing cells were transduced with the TKOv1 library, talazoparib was added on day 6 (t6; HeLa: 20 nM, RPE1-hTERT: 50 nM) and cells were cultured in its presence until day 18 (t18). Cells were subcultured once at day 12 (RPE1) or 13 (HeLa). sgRNA representations in the initial (t6) and final (t18) populations were quantified by next-generation sequencing. Gene knockouts that were enriched at t18 over t6 were identified by MAGeCK33. **b,** CRISPR-mediated inactivation of *RNASEH2A* and/or *PARP1* in cell lines used in **c-e** and Fig 3b. WCEs were processed for

immunoblotting with the indicated antibodies. KAP1, loading control. Representative of $n = 2$ biologically independent experiments. **c-e,** Loss of PARP1 restores PARPi-resistance in *RNASEH2A-KO* cells. **c,** Percentage of cleaved caspase-3+ HeLa cells of indicated genotypes with or without olaparib treatment measured by flow cytometry (FACS). Individual values (open circles) with mean (red lines, $n = 3$ biologically independent experiments; *P*-value, unpaired two-tailed t-test). **d,e.** Clonogenic survival assays with HeLa (**d**) and RPE1-hTERT (**e**) cells of the indicated genotypes treated with olaparib (left) or talazoparib (right). Mean ±SD ($n = 3$ biologically independent experiments). Solid lines, nonlinear least squares fit to a three-parameter dose response model. **f.** Trapping activity of PARPi correlates with the ability to induce apoptosis in *RNASEH2A-KO* cells. Quantification of cleaved caspase-3-positive HeLa WT and *RNASEH2B-KO* cells without treatment or treated with the indicated PARPi. Individual values with mean (black lines, $n = 3$ biologically independent experiments). Note that PARP-trapping activity decreases as follows: talazoparib > olaparib > veliparib 4,17. **g,** PARPi-induced S-phase arrest in *RNASEH2A-KO* cells is alleviated in the absence of PARP1. Top, schematic of talazoparib and EdU treatment. Bottom, representative ($n = 3$ biologically independent experiments) EdU (pseudocolor plots) and DNA content (histograms) FACS profiles of untreated and talazoparib-treated HeLa WT, *PARP1-KO*, *RNASEH2A-KO* and *PARP1-KO/RNASEH2A-KO* cells. DNA content was determined by propidium iodide (PI) staining. **h** Quantification of mean γ-H2AX intensities in experiments shown in Fig 3c. Individual values (open circles) with mean (red lines, $n = 3$ biologically independent experiments, 10,000 cells / sample / experiment analyzed).
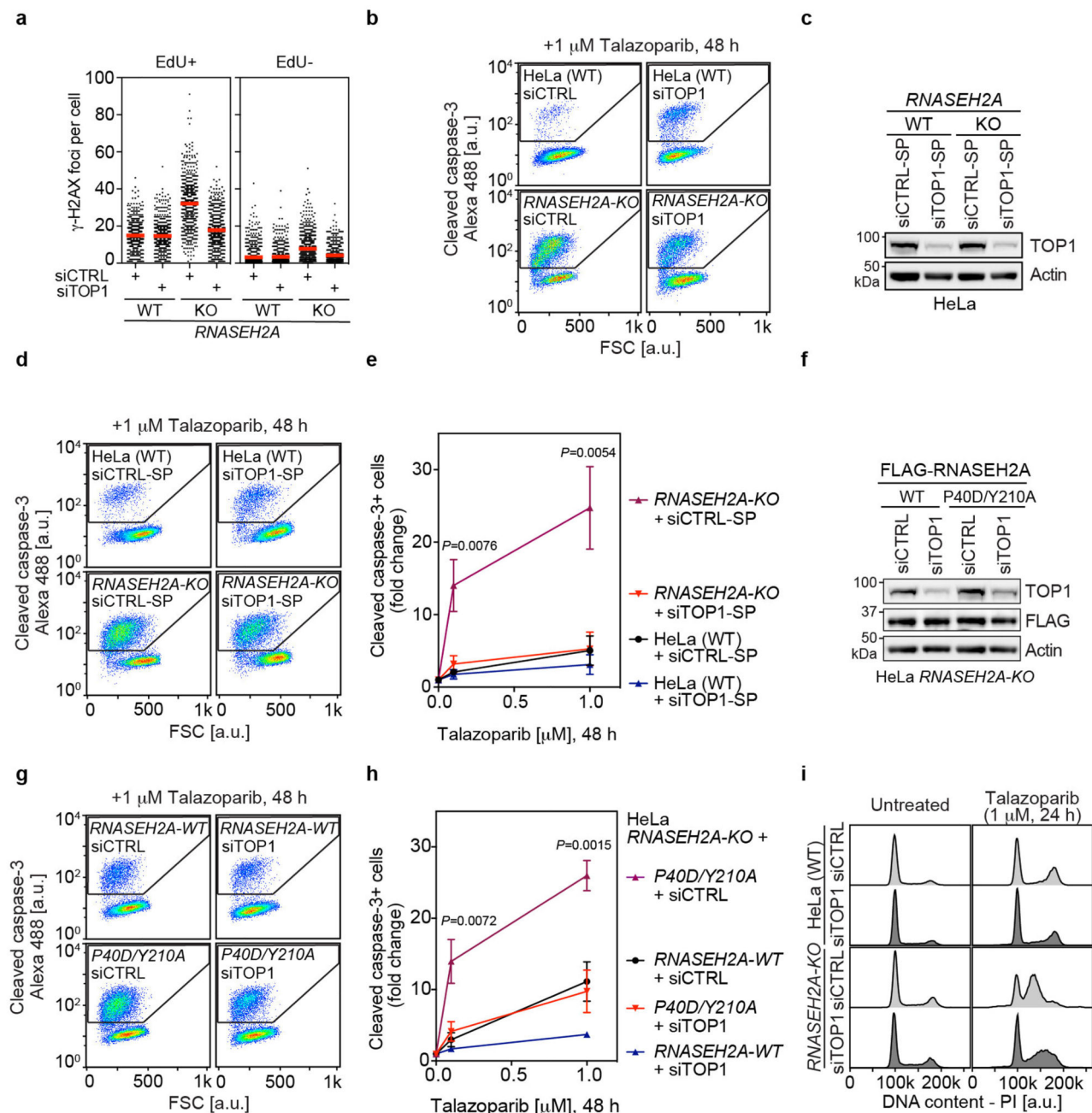
ED Figure 6.

Related to Figure 3d-g. TOP1-mediated cleavage at genome-embedded ribonucleotides leads to PARPi sensitivity in RER-deficient cells. a, Reduced endogenous DNA damage in TOP1-depleted *RNASEH2A-KO* cells. Quantification of γ-H2AX foci per nucleus in experiments shown in Fig 3e,f. Dots, focus number in individual nuclei. Red lines, mean (*n* = 5 biologically independent experiments). **b-i,** TOP1 depletion alleviates PARPi-induced apoptosis and S-phase arrest in HeLa *RNASEH2A-KO* cells (**b-e**) and in RNASEH2A P40D/Y210A separation-of-function mutant cells (**f-h**). **b,** Representative (*n* = 3 biologically

independent experiments) cleaved caspase-3 FACS plots for experiments quantified in Fig 3g. FSC, forward scatter. **c,** HeLa WT and *RNASEH2A-KO* cells were transfected with non-targeting (siCTRL-SP) or TOP1-targeting (siTOP1-SP) SMARTpool siRNAs. WCEs analyzed by immunoblotting with antibodies to TOP1 and actin (loading control). Representative of $n = 3$ biologically independent experiments. **d,** Representative ($n = 3$ biologically independent experiments) FACS plots of cleaved caspase-3 in siCTRL-SP or siTOP1-SP-transfected WT and *RNASEH2A-KO* HeLa cells after talazoparib treatment. FSC, forward scatter. **e,** Quantification of the experiment shown in **d**. **f,** HeLa *RNASEH2A-KO* cells stably expressing the indicated FLAG-tagged constructs were transfected with non-targeting (siCTRL) or TOP1-targeting (siTOP1) siRNAs. WCEs were analyzed by immunoblotting with antibodies to TOP1, FLAG and actin (loading control). Representative of $n = 3$ biologically independent experiments. **g,** Representative ($n = 3$ biologically independent experiments) FACS plots of cleaved caspase-3 in siCTRL- or siTOP1-transfected HeLa *RNASEH2A-KO* cells expressing RNASEH2A-WT or P40D/Y210A mutant. **h**, Quantification of the experiment shown in **g**. Data in **e,h,** mean ±SD normalized to untreated cells ($n = 3$ biologically independent experiments, 10,000 cells / sample / experiment analyzed; *P* values, unpaired two-tailed t-test). **i,** Representative ($n = 3$ biologically independent experiments**)** cell cycle profiles, prior and post talazoparib treatment, of HeLa WT and *RNASEH2A-KO* cells transfected with the indicated siRNAs. DNA content was assessed by PI staining and FACS.

ED Figure 7.

Related to Figure 4a-c. Collateral loss of *RNASEH2B* in CLL and metastatic castration-resistant prostate cancer (CRPC). a, b, Multiplex ligation-dependent probe amplification (MLPA) analysis (**a**) and comparative genomic hybridization (CGH) array profiles for chromosome 13q (**b**) of representative CLL samples carrying two wild-type (WT) *RNASEH2B* alleles (top), a monoallelic *RNASEH2B* deletion (middle) or biallelic deletion (bottom). **a,** For MLPA analysis, genomic DNA from reference and experimental samples was analyzed using probes targeting control loci and individual *RNASEH2B* exons

(Exon 1-11). MLPA ratio calculated per probe and normalised to control probes and reference samples. Error bars indicate SD of the mean from 8 control probes for each sample. Dashed lines indicate the threshold set for diploid copy number. **b**, For each CGH array profile the y-axes of the top and bottom plots indicate copy number probe intensity (log R ratio) and the x axes mark the position on chromosome 13 represented by the ideogram (middle). An enlargement of the frequently deleted 13q14.2-14.3 region, including the *miRNA-15A/16-1* gene cluster and the *RNASEH2B* gene, is shown in the bottom plot. *n* = 1 experiment. **c**, *RNASEH2B* is frequently co-deleted with *RB1* in CRPC. Copy number alterations (CNA) in the *RB1-RNASEH2B* region in CRPC (n = 226 cases) are shown. Horizontal lines represent the CNA profile for individual CRPC samples (dark blue, homozygous loss; light blue, heterozygous loss; grey, no change; pink, copy number gain (CNA 3-4); red, copy number amplification (CNA > 4); white, insufficient data to determine CNA). Samples are clustered based on *RNASEH2B* gene status. CNA frequencies for *RNASEH2B* and the *RB1-RNASEH2B* region without a copy number breakpoint are shown on the right.
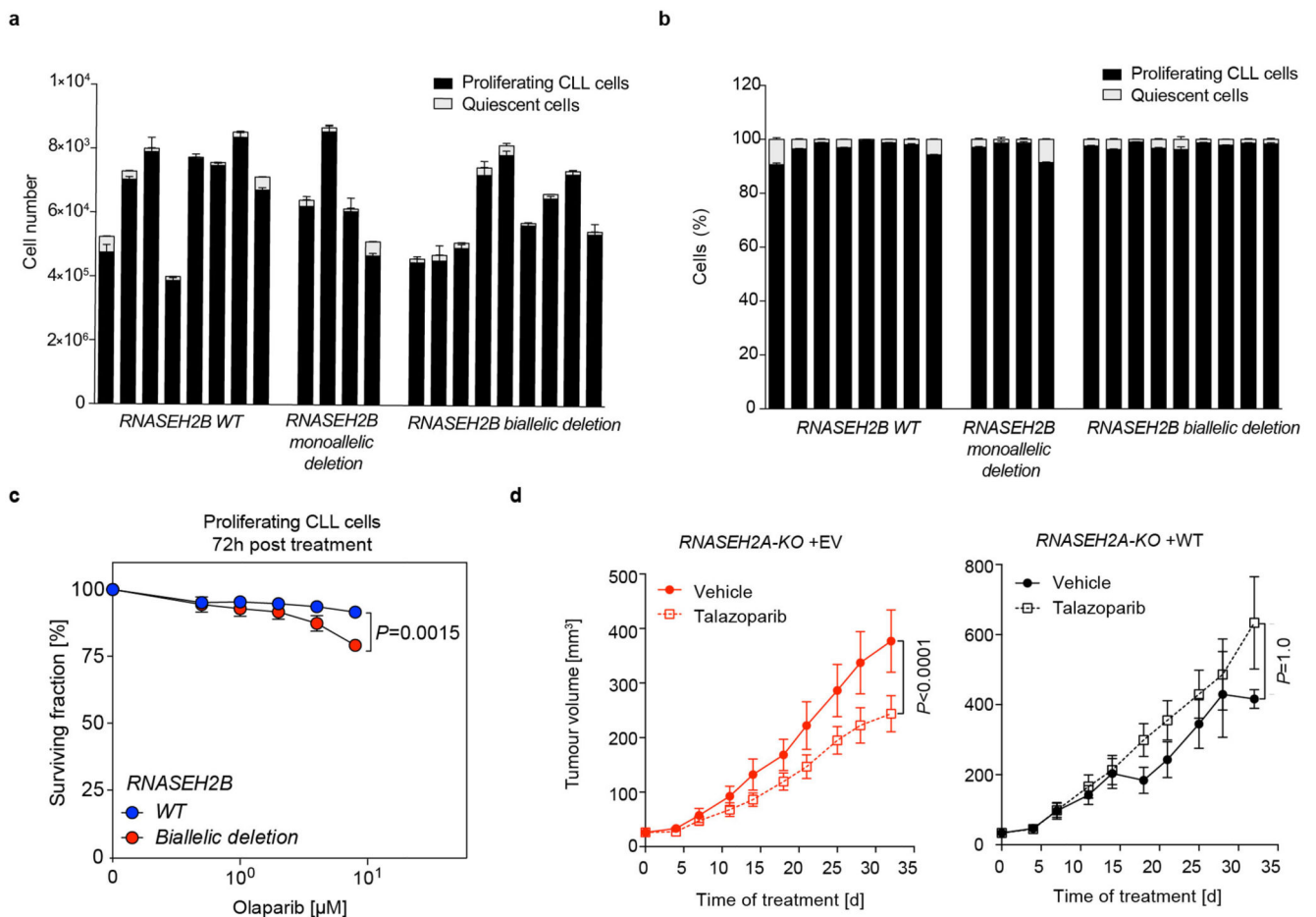
ED Figure 8.
Related to Figure 4. a,b, Proliferating cells, and not quiescent cells, are the major population of viable cells in *ex-vivo* cultured primary CLL patient samples irrespective of

treatment group. Quantification of absolute (**a**) and relative (**b**) quiescent and proliferating cell numbers as determined by FACS analysis of the primary CLL samples used in Fig 4b,c. (*RNASEH2B* WT, $n = 8$ individual samples; monoallelic deletion, $n = 4$ individual samples; biallelic deletion, $n = 9$ individual samples). Mean ± SD ($n = 3$ technical replicate). FACS gating strategy for stimulated peripheral blood lymphocytes (PBLs) from CLL patients is shown in Supplementary Fig 2. **c**, RNase H2-deficient primary CLL cells have reduced survival when cultured with olaparib. Mean of individual samples ± s.e.m. ($n = 3$ biologically independent CLL samples / group, each analyzed in technical triplicates). *P*-value, two-way ANOVA. **d,** Talazoparib selectively inhibits the growth of *RNASEH2A-KO* xenograft tumours. *RNASEH2A-KO* cells complemented either with empty vector (EV) or RNASEH2A-WT were injected subcutaneously into bilateral flanks of CD-1 nude mice. Mice were randomized to either vehicle or talazoparib (0.333 mg/kg) treatment groups (n = 8 animals / group) and tumour volumes were measured twice-weekly. Data plotted as mean ± s.e.m. *P*-values. two-way ANOVA under the null hypothesis that talazoparib does not supress the tumour growth.
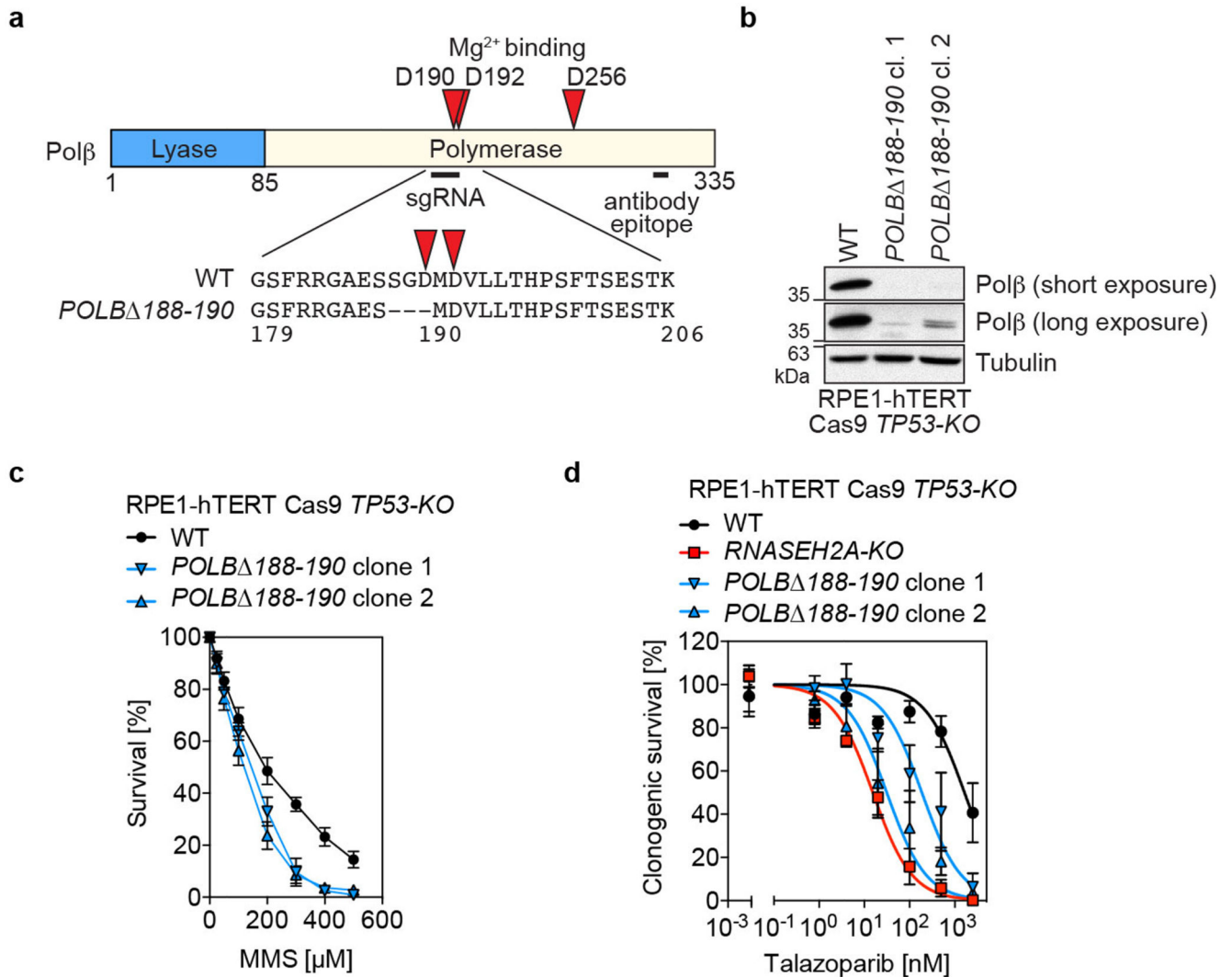
ED Figure 9.

RNase H2-deficient cells are more sensitive to PARPi than DNA polymerase β mutants.

a, Schematic representation of the *POLBΔ188-190* CRISPR mutation. The Mg^{2+}-coordinating aspartate residues (D190, D192 and D256, red triangles) are highlighted in the domain structure of the human Polβ protein. The sgRNA target site and antibody epitope are indicated by black lines. **b,** WCEs from parental RPE1-hTERT Cas9 *TP53-KO* cells and two *POLBΔ188-190* clones were processed for immunoblotting with antibodies to Polβ and tubulin (loading control). Representative of $n = 2$ biologically independent experiments. **c,** The *POLBΔ188-190* mutation impairs base excision repair. RPE1-hTERT Cas9 *TP53-KO* WT or *POLBΔ188-190* cells were exposed to different concentrations of methyl-methanesulfonate (MMS) for 24 h, followed by growth in drug-free media for an additional 48 h. Cell viability was determined by the Cell Titer Glo assay. **d,** Sensitivity of RPE1-hTERT Cas9 *TP53-KO* WT, *RNASEH2A-KO* and *POLBΔ188-190* cells to indicated talazoparib concentrations in clonogenic survival assays. Data in **c** and **d** represent mean

±SD, normalized to untreated cells ($n = 3$ biologically independent experiments). Solid lines denote a nonlinear least-squares fit to a three-parameter dose response model.

Extended Data Table 1

Clinical and molecular characteristics of primary CLL samples used in Fig. 4b,c, ED Fig. 7a,b and ED Fig. 8a,b

See table for details.

	Clinical characteristics								Molecular characteristics			
Sample	Age	Sex	Binet stage	Time from diagnosis (Months)	Treatment	Time on treatment (Days)	Response to treatment	Cytogenetics (FISH)	RNASEH2B status[1]	ATM status[2]	TP53 status[3]	IgVH status[4]
CLL1	67	F	A	35	Pre-treatment	0	-	Trisomy 12	WT	WT	WT	M
CLL2	74	F	A	24	Pre-treatment	0	-	Normal	WT	WT	c.658_663del, c.849_850insC#	UM
CLL3	67	M	A	176	Ibrutinib	0	PRL	Normal	WT	WT	WT	UM
CLL4	68	M	A	49	Pre-treatment	0	-	Normal	WT	WT	WT	M
CLL5	76	M	A	49	Pre-treatment	0	-	N/A	WT	WT	WT	UM
CLL6	65	F	A	153	Pre-treatment	0	-	N/A	WT	WT	WT	M
CLL7	63	F	A	199	Fludarabine +Cyclophosphamide +Rituximab	37	CR	Trisomy 12	WT	WT	WT	UM
CLL8	39	M	B	80	Pre-treatment	0	-	Normal	WT	WT	WT	M
CLL9	80	F	A	33	Chlorambucil	83	PR	del(13q)	Monoallelic del	WT	WT	M
CLL10	57	F	A	136	Pre-treatment	0	-	del(13q)	Monoallelic del	WT	WT	M
CLL11	79	F	A	70	Bendamustine + rituximab	251	CR	N/A	Monoallelic del	WT	WT	M
CLL12	48	M	B	159	Ibrutinib	486	PR	N/A	Monoallelic del	WT	WT	UM
CLL13	62	F	A	203	Pre-treatment	0	-	N/A	Biallelic del	WT	WT	M
CLL14	63	M	A	27	Pre-treatment	0	-	del(13q)	Biallelic del	WT	WT	UM
CLL15	42	F	A	414	Bendamustine + rituximab +/- ibrutinib	120	SD	del(13q)	Biallelic del	WT	c.561A>G *	M
CLL16	84	F	A	19	Pre-treatment	0	-	N/A	Biallelic del	WT	WT	M
CLL17	72	F	A	153	Chlorambucil	63	PR	Trisomy 12, del(13q)	Biallelic del	WT	c.743G>A *	M
CLL18	79	F	A	36	Pre-treatment	0	-	del(13q)	Biallelic del	WT	WT	M
CLL19	48	F	B	8	Pre-treatment	0	-	del(17p), del(13q)	Biallelic del	WT	c.753_754insCC#	M
CLL20	70	F	B	10	Pre-treatment	0	-	del(13q)	Biallelic del	WT	WT	UM

	Clinical characteristics						Molecular characteristics			
Sample	Age	Sex	Binet stage	Time from diagnosis (Months)	Treatment	Time on treatment (Days)	Response to treatment	Cytogenetics (FISH)	RNASEH2B status[1]	ATM status[2]	TP53 status[3]	IgVH status[4]
CLL21	67	M	B	56	Pre-treatment	0	-	del(13q)	Biallelic del	WT	WT	UM

CLL samples grouped by *RNASEH2B* status. F, female; M, male; PRL, partial response with lymphocytosis; SD, stable disease; PR, partial response; CR, complete response; "-", not applicable; N/A, not available; WT. [1] Based on MLPA and CGH array, WT, wild-type; del, deleted; [2] WT, intact ATM status confirmed by next-generation sequencing (NGS) and/or functional assays; [3] *TP53* status determined by sequencing, WT, no mutations in coding sequencing; otherwise mutation(s) shown, * monoallelic *TP53* alteration, # biallelic *TP53* alteration. [4] Maturational status of CLL assessed by detection of hypermutation in Immunoglobulin Heavy chain variable region (IgVH); UM, ummutated >98% sequence homology with germline sequence; M, mutated <98% sequence homology with germline sequence.

Supplementary Material

Refer to Web version on PubMed Central for supplementary material.

Acknowledgements

References

1. Lord CJ, Ashworth A. PARP inhibitors: Synthetic lethality in the clinic. Science. 2017; 355:1152–1158. DOI: 10.1126/science.aam7344 [PubMed: 28302823]

2. Pommier Y, O'Connor MJ, de Bono J. Laying a trap to kill cancer cells: PARP inhibitors and their mechanisms of action. Sci Transl Med. 2016; 8:362ps317.doi: 10.1126/scitranslmed.aaf9246

3. Hopkins TA, et al. Mechanistic Dissection of PARP1 Trapping and the Impact on In Vivo Tolerability and Efficacy of PARP Inhibitors. Molecular cancer research : MCR. 2015; 13:1465–1477. DOI: 10.1158/1541-7786.MCR-15-0191-T [PubMed: 26217019]

4. Murai J, et al. Trapping of PARP1 and PARP2 by Clinical PARP Inhibitors. Cancer Res. 2012; 72:5588–5599. DOI: 10.1158/0008-5472.CAN-12-2753 [PubMed: 23118055]

5. Cerritelli SM, Crouch RJ. The Balancing Act of Ribonucleotides in DNA. Trends Biochem Sci. 2016; 41:434–445. DOI: 10.1016/j.tibs.2016.02.005 [PubMed: 26996833]

6. Elstrodt F, et al. BRCA1 mutation analysis of 41 human breast cancer cell lines reveals three new deleterious mutants. Cancer Res. 2006; 66:41–45. DOI: 10.1158/0008-5472.CAN-05-2853 [PubMed: 16397213]

7. Daemen A, et al. Cross-platform pathway-based analysis identifies markers of response to the PARP inhibitor olaparib. Breast Cancer Res Treat. 2012; 135:505–517. DOI: 10.1007/s10549-012-2188-0 [PubMed: 22875744]

8. Wang G, et al. Identifying drug-gene interactions from CRISPR knockout screens with drugZ. bioRxiv. 2017; doi: 10.1101/232736

9. Ohle C, et al. Transient RNA-DNA Hybrids Are Required for Efficient Double-Strand Break Repair. Cell. 2016; 167:1001–1013 e1007. DOI: 10.1016/j.cell.2016.10.001 [PubMed: 27881299]

10. Pierce AJ, Johnson RD, Thompson LH, Jasin M. XRCC3 promotes homology-directed repair of DNA damage in mammalian cells. Genes Dev. 1999; 13:2633–2638. [PubMed: 10541549]

11. Potenski CJ, Niu H, Sung P, Klein HL. Avoidance of ribonucleotide-induced mutations by RNase H2 and Srs2-Exo1 mechanisms. Nature. 2014; 511:251–254. DOI: 10.1016/j.cell.2016.10.001 [PubMed: 24896181]

12. Pizzi S, et al. Reduction of hRNase H2 activity in Aicardi-Goutieres syndrome cells leads to replication stress and genome instability. Human molecular genetics. 2015; 24:649–658. DOI: 10.1093/hmg/ddu485 [PubMed: 25274781]

13. Reijns MA, et al. Enzymatic removal of ribonucleotides from DNA is essential for mammalian genome integrity and development. Cell. 2012; 149:1008–1022. DOI: 10.1016/j.cell.2012.04.011 [PubMed: 22579044]

14. Hiller B, et al. Mammalian RNase H2 removes ribonucleotides from DNA to maintain genome integrity. J Exp Med. 2012; 209:1419–1426. DOI: 10.1084/jem.20120876 [PubMed: 22802351]

15. Reijns MA, Jackson AP. Ribonuclease H2 in health and disease. Biochemical Society transactions. 2014; 42:717–725. DOI: 10.1042/BST20140079 [PubMed: 25109948]

16. Chon H, et al. RNase H2 roles in genome integrity revealed by unlinking its activities. Nucleic Acids Res. 2013; 41:3130–3143. DOI: 10.1093/nar/gkt027 [PubMed: 23355612]

17. Murai J, et al. Stereospecific PARP trapping by BMN 673 and comparison with olaparib and rucaparib. Mol Cancer Ther. 2014; 13:433–443. DOI: 10.1158/1535-7163.MCT-13-0803 [PubMed: 24356813]

18. Kim N, et al. Mutagenic processing of ribonucleotides in DNA by yeast topoisomerase I. Science. 2011; 332:1561–1564. DOI: 10.1126/science.1205016 [PubMed: 21700875]

19. Sparks JL, Burgers PM. Error-free and mutagenic processing of topoisomerase 1-provoked damage at genomic ribonucleotides. EMBO J. 2015; 34:1259–1269. DOI: 10.15252/embj.201490868 [PubMed: 25777529]

20. Williams JS, et al. Topoisomerase 1-mediated removal of ribonucleotides from nascent leading-strand DNA. Mol Cell. 2013; 49:1010–1015. DOI: 10.1016/j.molcel.2012.12.021 [PubMed: 23375499]

21. Sekiguchi J, Shuman S. Site-specific ribonuclease activity of eukaryotic DNA topoisomerase I. Mol Cell. 1997; 1:89–97. [PubMed: 9659906]

22. Pommier Y, Sun Y, Huang SN, Nitiss JL. Roles of eukaryotic topoisomerases in transcription, replication and genomic stability. Nat Rev Mol Cell Biol. 2016; 17:703–721. DOI: 10.1038/nrm. 2016.111 [PubMed: 27649880]

23. Huang SN, Williams JS, Arana ME, Kunkel TA, Pommier Y. Topoisomerase I-mediated cleavage at unrepaired ribonucleotides generates DNA double-strand breaks. EMBO J. 2017; 36:361–373. DOI: 10.15252/embj.201592426 [PubMed: 27932446]

24. Kipps TJ, et al. Chronic lymphocytic leukaemia. Nat Rev Dis Primers. 2017; 3:16096.doi: 10.1038/nrdp.2016.96 [PubMed: 28102226]

25. Klein U, et al. The DLEU2/miR-15a/16-1 cluster controls B cell proliferation and its deletion leads to chronic lymphocytic leukemia. Cancer Cell. 2010; 17:28–40. DOI: 10.1016/j.ccr.2009.11.019 [PubMed: 20060366]

26. Cancer Genome Atlas Research, N. The Molecular Taxonomy of Primary Prostate Cancer. Cell. 2015; 163:1011–1025. DOI: 10.1016/j.cell.2015.10.025 [PubMed: 26544944]

27. Mu P, et al. SOX2 promotes lineage plasticity and antiandrogen resistance in TP53- and RB1-deficient prostate cancer. Science. 2017; 355:84–88. DOI: 10.1126/science.aah4307 [PubMed: 28059768]

28. Ku SY, et al. Rb1 and Trp53 cooperate to suppress prostate cancer lineage plasticity, metastasis, and antiandrogen resistance. Science. 2017; 355:78–83. DOI: 10.1126/science.aah4199 [PubMed: 28059767]

29. Armenia J, et al. The long tail of oncogenic drivers in prostate cancer. Nat Genet. 2018; doi: 10.1038/s41588-018-0078-z

30. Hart T, et al. High-Resolution CRISPR Screens Reveal Fitness Genes and Genotype-Specific Cancer Liabilities. Cell. 2015; 163:1515–1526. DOI: 10.1016/j.cell.2015.11.015 [PubMed: 26627737]

31. Reijns MA, et al. The structure of the human RNase H2 complex defines key interaction interfaces relevant to enzyme function and human disease. J Biol Chem. 2011; 286:10530–10539. DOI: 10.1074/jbc.M110.177394 [PubMed: 21177854]

32. Sakaue-Sawano A, et al. Visualizing spatiotemporal dynamics of multicellular cell-cycle progression. Cell. 2008; 132:487–498. S0092-8674(08)00054-8 [pii]. DOI: 10.1016/j.cell. 2007.12.033 [PubMed: 18267078]

33. Li W, et al. MAGeCK enables robust identification of essential genes from genome-scale CRISPR/Cas9 knockout screens. Genome Biol. 2014; 15:554.doi: 10.1186/s13059-014-0554-4 [PubMed: 25476604]

34. Bunz F, et al. Requirement for p53 and p21 to sustain G2 arrest after DNA damage. Science. 1998; 282:1497–1501. [PubMed: 9822382]

35. Swift S, Lorens J, Achacoso P, Nolan GP. Rapid production of retroviruses for efficient gene delivery to mammalian cells using 293T cell-based systems. Curr Protoc Immunol. 2001; Chapter 10 Unit 10 17C. doi: 10.1002/0471142735.im1017cs31

36. Ran FA, et al. Genome engineering using the CRISPR-Cas9 system. Nat Protoc. 2013; 8:2281–2308. DOI: 10.1038/nprot.2013.143 [PubMed: 24157548]

37. Sanjana NE, Shalem O, Zhang F. Improved vectors and genome-wide libraries for CRISPR screening. Nat Methods. 2014; 11:783–784. DOI: 10.1038/nmeth.3047 [PubMed: 25075903]

38. Solier S, et al. Genome-wide analysis of novel splice variants induced by topoisomerase I poisoning shows preferential occurrence in genes encoding splicing factors. Cancer Res. 2010; 70:8055–8065. DOI: 10.1158/0008-5472.CAN-10-2491 [PubMed: 20817775]

39. Naughton C, et al. Transcription forms and remodels supercoiling domains unfolding large-scale chromatin structures. Nat Struct Mol Biol. 2013; 20:387–395. DOI: 10.1038/nsmb.2509 [PubMed: 23416946]

40. Helmrich A, Ballarino M, Tora L. Collisions between replication and transcription complexes cause common fragile site instability at the longest human genes. Mol Cell. 2011; 44:966–977. DOI: 10.1016/j.molcel.2011.10.013 [PubMed: 22195969]

41. Puc J, et al. Ligand-dependent enhancer activation regulated by topoisomerase-I activity. Cell. 2015; 160:367–380. DOI: 10.1016/j.cell.2014.12.023 [PubMed: 25619691]

42. Harley ME, et al. TRAIP promotes DNA damage response during genome replication and is mutated in primordial dwarfism. Nat Genet. 2016; 48:36–43. DOI: 10.1038/ng.3451 [PubMed: 26595769]

43. Brinkman EK, Chen T, Amendola M, van Steensel B. Easy quantitative assessment of genome editing by sequence trace decomposition. Nucleic Acids Res. 2014; 42:e168.doi: 10.1093/nar/gku936 [PubMed: 25300484]

44. Mi H, Muruganujan A, Thomas PD. PANTHER in 2013: modeling the evolution of gene function, and other gene attributes, in the context of phylogenetic trees. Nucleic Acids Res. 2013; 41:D377–386. DOI: 10.1093/nar/gks1118 [PubMed: 23193289]

45. Reynolds JJ, et al. Mutations in DONSON disrupt replication fork stability and cause microcephalic dwarfism. Nat Genet. 2017; 49:537–549. DOI: 10.1038/ng.3790 [PubMed: 28191891]

46. Escribano-Diaz C, et al. A Cell Cycle-Dependent Regulatory Circuit Composed of 53BP1-RIF1 and BRCA1-CtIP Controls DNA Repair Pathway Choice. Molecular cell. 2013; 49:872–883. DOI: 10.1016/j.molcel.2013.01.001 [PubMed: 23333306]

47. Pascutti MF, et al. IL-21 and CD40L signals from autologous T cells can induce antigen-independent proliferation of CLL cells. Blood. 2013; 122:3010–3019. DOI: 10.1182/blood-2012-11-467670 [PubMed: 24014238]

48. Robinson D, et al. Integrative clinical genomics of advanced prostate cancer. Cell. 2015; 161:1215–1228. DOI: 10.1016/j.cell.2015.05.001 [PubMed: 26000489]
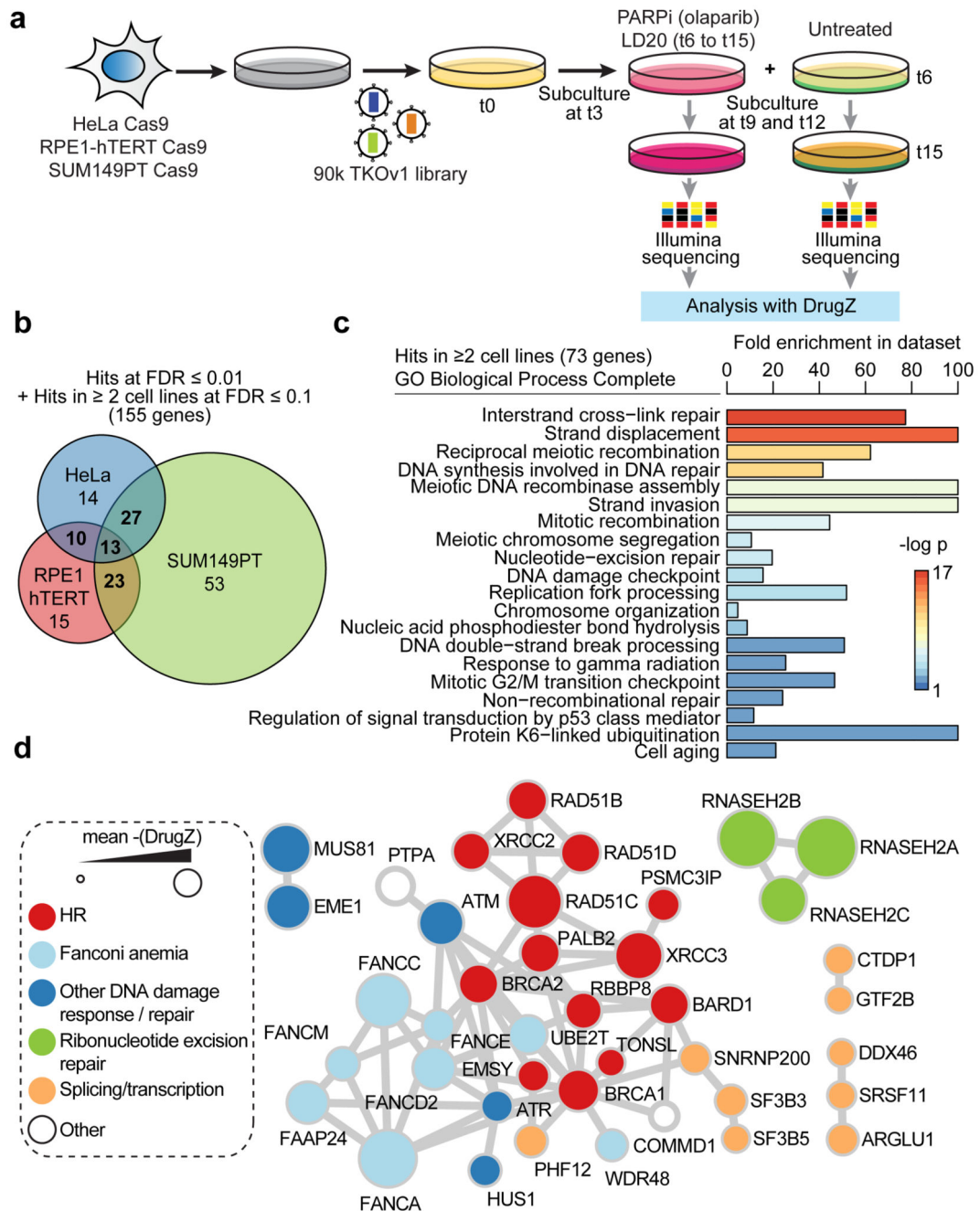
Figure 1. CRISPR screens identify determinants of PARP inhibitor (PARPi) sensitivity.
a, Schematic of screening pipeline. **b,** Venn diagram of all high-confidence hits (FDR 0.01 + FDR 0.1 in 2 cell lines) in individual cell lines. **c,** Gene ontology (GO) terms significantly ($P < 0.05$, binomial test with Bonferroni correction) enriched among hits common to 2 cell lines. **d,** esyN network analysis of interactions between hits common to 2 cell lines. Node size represents the mean DrugZ score across cell lines. 31/73 genes are mapped on the network. See also ED Fig 1.
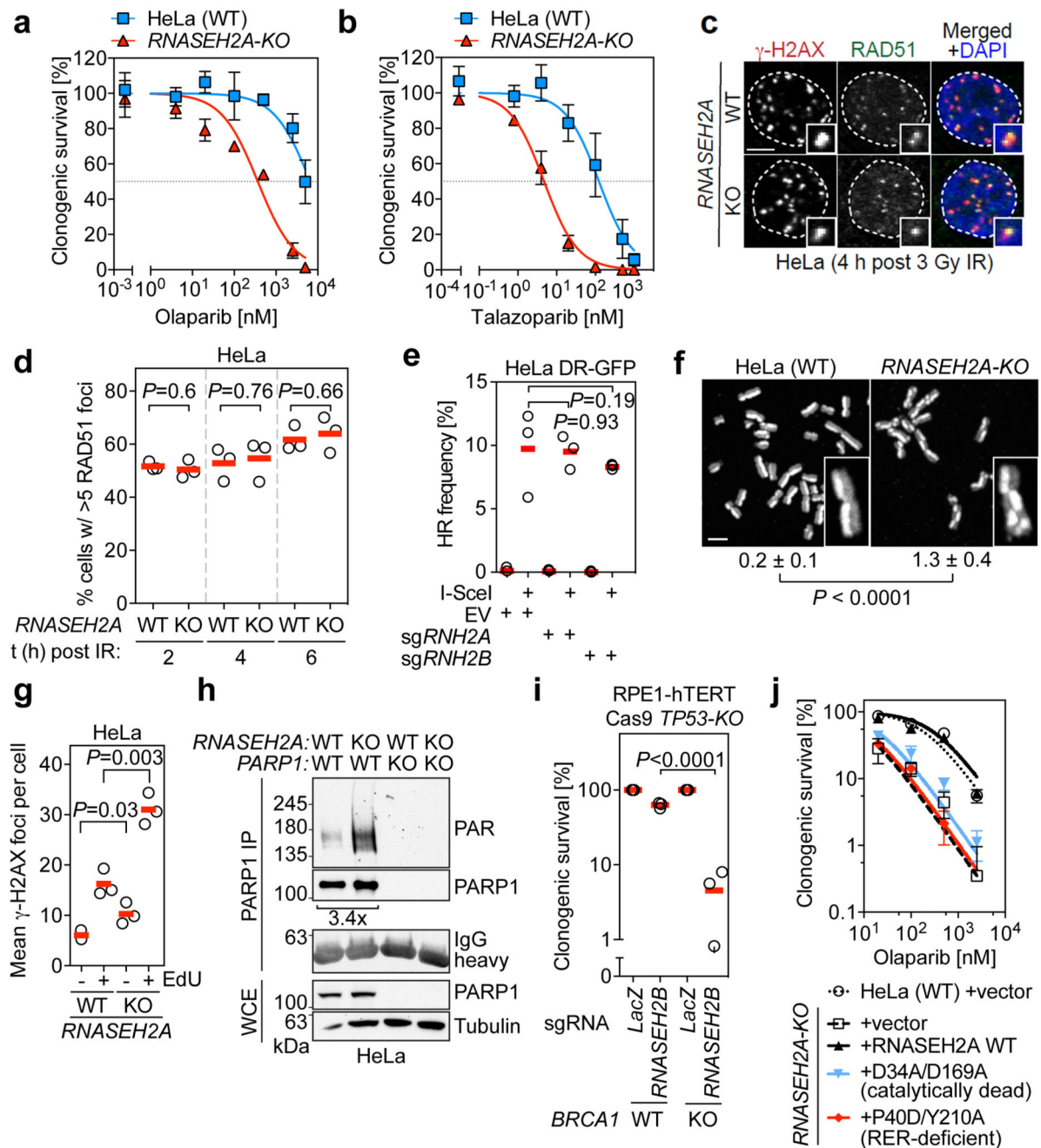
Figure 2. Defective ribonucleotide excision repair causes PARPi sensitivity, DNA damage and synthetic lethality with BRCA1 deficiency.

a,b, Reduced survival of HeLa *RNASEH2A-KO* cells after treatment with indicated PARPi. Mean ±SD, normalized to untreated cells. Solid lines, nonlinear least-squares fit to a three-parameter dose-response model. **c-f,** *RNASEH2A-KO* cells are HR-proficient. **c,d,** Normal RAD51 focus formation in *RNASEH2A-KO* HeLa cells after X-ray exposure. **c,** Representative micrographs of HeLa WT and *RNASEH2A-KO* cells stained with indicated antibodies (*n* = 3 biologically independent experiments). Scale bar, 10 μm. **d,** Quantification.

Percentage of cells with >5 RAD51/γ-H2AX colocalizing foci at indicated time points. **e,** HR is not impaired in RNase H2-null cells. Quantification of gene conversion in DR-GFP reporter cells11 transduced with Cas9 + sg*RNASEH2A/B* or empty vector (EV) ± I-SceI transfection. Values normalized to transfection efficiency of control GFP vector. **f,** Increased sister chromatid exchanges (SCEs) in *RNASEH2A-KO* cells. Representative micrographs of SCEs in WT and *RNASEH2A-KO* metaphases. Below, numbers of SCEs / chromosome (mean ±SD, *n* = 3 biologically independent experiments). Scale bars, 10 μm. **g,h,** Spontaneous replication-associated damage and increased PARP1 activation in *RNASEH2A-KO* cells. **g,** Quantification of mean γ-H2AX immunofluorescent foci number / nucleus in EdU positive (+) and -negative (-) WT and *RNASEH2A-KO* cells. **h,** Representative poly(ADP-ribose) (PAR) immunoblot of PARP1 immunoprecipitates (IP) from whole cell extracts (WCE). Mean fold-increase in PARylation between WT and *RNASEH2A-KO* indicated (*n* = 3 biologically independent experiments, normalized to immunoprecipitated PARP1 levels). Tubulin and IgG heavy chain, loading controls. **i,** Synthetic lethality in combined absence of RNase H2 and BRCA1. Quantification of colony formation of *BRCA1*-proficient (WT) and *BRCA1-KO* RPE1-hTERT Cas9 *TP53-KO* cells transduced with sg*LacZ* or sg*RNASEH2B* constructs. Open circles, individual values normalized to sg*LacZ*; red lines, mean (*n* = 3 biologically independent experiments). **j,** PARPi sensitivity is associated with ribonuclease excision repair (RER) deficiency. Survival of olaparib-treated HeLa WT and *RNASEH2A-KO* cells transduced with indicated FLAG-tagged constructs. Mean ±SD, normalized to untreated cells (*n* = 3 biologically independent experiments). Solid lines, nonlinear least squares fit to a three-parameter dose response model. For **d**, **e**, and **g**: open circles, individual values; red lines, mean [*n* = 3 biologically independent experiments; 100 (**d, g**) and 1000 (**e**) cells / sample / experiment analyzed]. *P* values in **d-g** and **i**, unpaired two-tailed t-test. See also ED Fig 2-4.
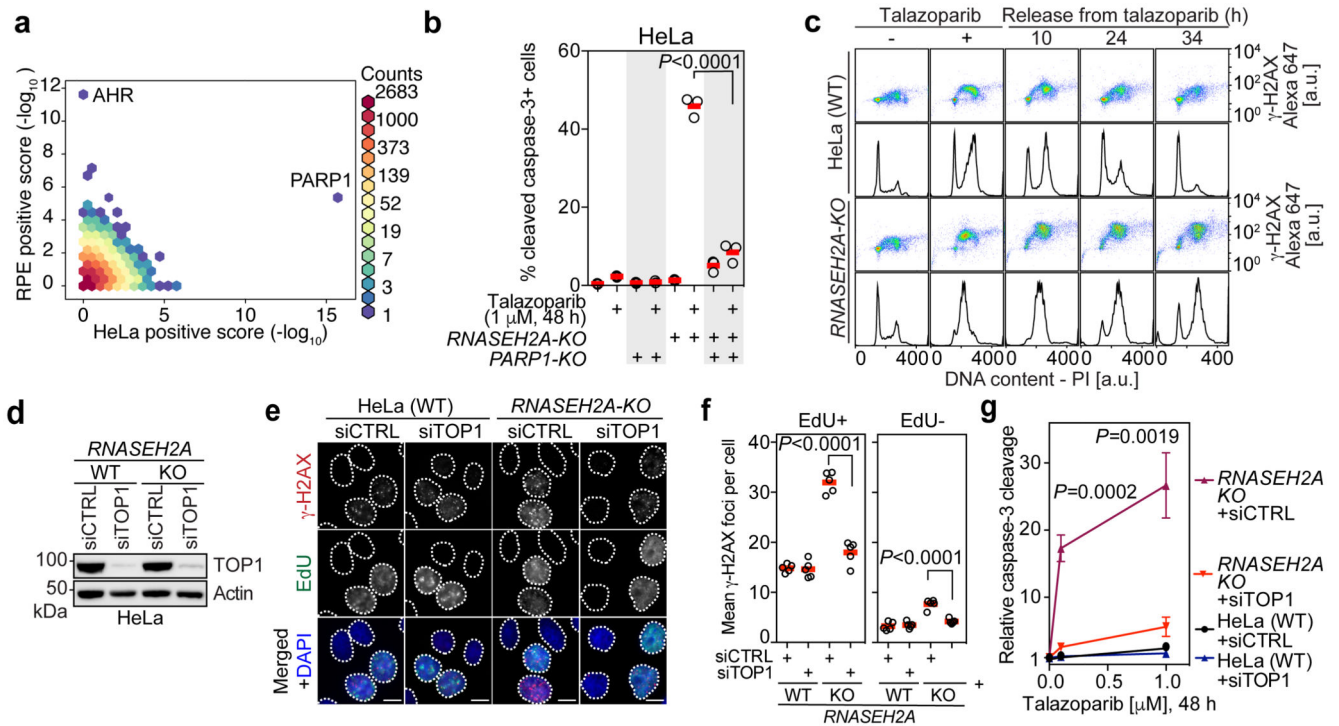
Figure 3. PARPi-induced PARP1 trapping occurs in RER-deficient cells as a result of TOP1-mediated processing of genomic ribonucleotides.

a,b, PARP1 is required for PARPi-induced toxicity in *RNASEH2A-KO* cells. CRISPR screens for talazoparib sensitivity suppressors in *RNASEH2A*-deficient HeLa Cas9 and RPE1 Cas9 *TP53-KO* cell lines. MAGeCK positive scores for each gene plotted. Colors indicate gene density in each hexagonal bin. **b,** Percentage of cleaved caspase-3+ cells of indicated genotypes with or without talazoparib treatment measured by flow cytometry (FACS). Open circles, individual experiments; red lines, mean ($n = 3$ biologically independent experiments). **c.** DNA damage persists on withdrawal of PARPi in *RNASEH2A-KO* cells. HeLa WT and *RNASEH2A-KO* cells were treated with talazoparib and released into fresh medium for the indicated times before being processed for γ-H2AX immunofluorescence and propidium iodide (PI) staining. Representative ($n = 3$ biologically independent experiments) γ-H2AX (pseudocolor plots) and cell cycle (histograms) IF/FACS profiles shown. **d-f,** Increased γ-H2AX foci formation in *RNASEH2A-KO* cells depends on TOP1 (images representative of $n = 5$ biologically independent experiments). **d,** HeLa WT and *RNASEH2A-KO* cells were transfected with non-targeting (siCTRL) or TOP1-targeting (siTOP1) siRNAs. Immunoblot of WCEs, probed for TOP1. Actin, loading control. **e,** Representative micrographs of HeLa WT and *RNASEH2A-KO* cells transfected with siCTRL or siTOP1 immunostained for γ-H2AX. Scale bars, 10 μm. **f,** Quantification of experiments shown in **e**. Mean number of foci / nucleus / experiment (open circles) with mean of $n = 5$ biologically independent experiments (red lines). 100 cells / sample / experiment analyzed. **g,** TOP1 depletion alleviates PARPi-induced apoptosis in *RNASEH2A-KO* cells. Quantification of cleaved caspase-3+ WT and *RNASEH2A-KO* cells transfected with indicated siRNAs, with or without talazoparib treatment. Mean ± SD

normalized to untreated cells ($n = 3$ biologically independent experiments). 10,000 cells / sample / experiment. *P* values in **b**, **f**, **g**, unpaired two-tailed t-test. See also ED Fig 5 and 6.
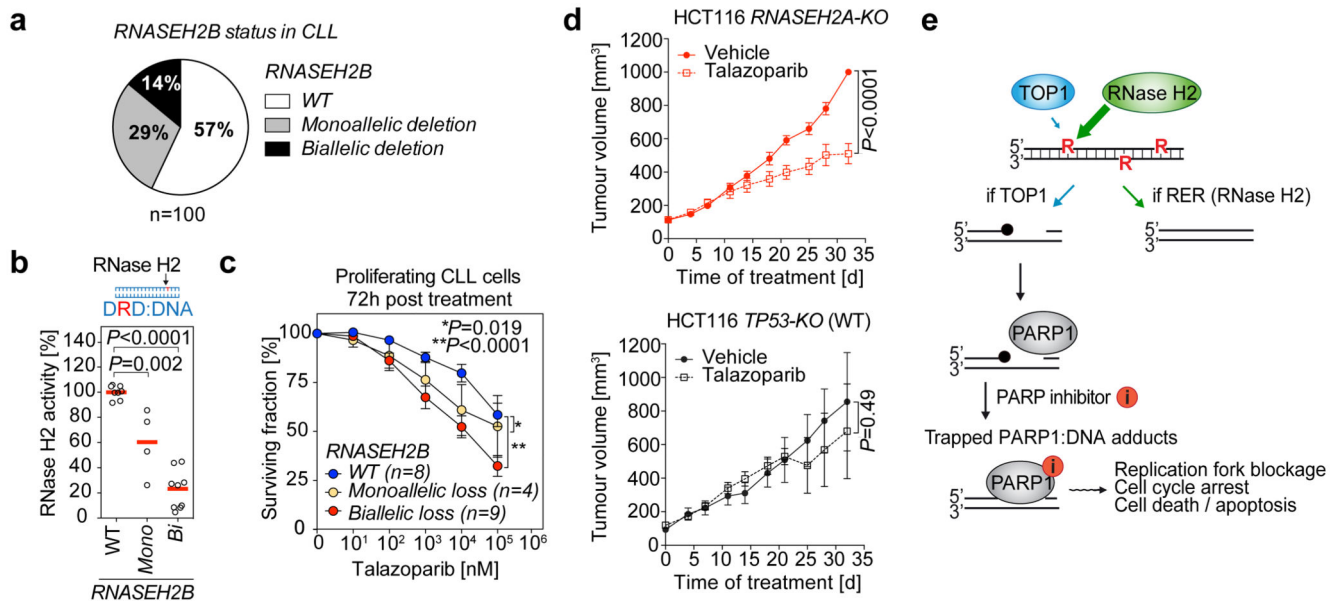
Figure 4. Talazoparib selectively suppresses growth of RNase H2 deficient tumours.
a-c, PARP inhibitors selectively kill *RNASEH2B*-deficient chronic lymphocytic leukemia (CLL) primary cancer cells. **a,** *RNASEH2B* deletion frequency in a panel of 100 primary CLL samples, determined by multiplex ligation-dependent probe amplification (MLPA). **b,** Reduced RNase H2 activity in lysates from CLL samples with monoallelic and biallelic *RNASEH2B* deletions. Top, substrate schematic. Individual data points, mean of technical duplicates for each sample. Red lines, mean of individual genotypes ($n = 8$ WT, 4 monoallelic and 9 biallelic deleted biologically independent primary CLL samples). Data normalized to mean of *RNASEH2B-WT* samples. **c,** Reduced survival of CLL cells with monoallelic and biallelic *RNASEH2B* loss following treatment with talazoparib. Individual points, mean ± s.e.m. ($n = 8$, 4 and 9 CLL samples as in **b**), each analysed in technical triplicates. *P*-values, unpaired two-tailed t-test (**b**) and two-way ANOVA (**c**). **d,** Selective inhibition of *RNASEH2A-KO* xenograft tumour growth. HCT116 *TP53-KO RNASEH2A-WT* or *-KO* cells were injected subcutaneously into bilateral flanks of CD-1 nude mice. Mice were randomized to either vehicle or talazoparib (0.333 mg/kg) treatment groups ($n = 8$ animals / group) and tumour volumes measured twice-weekly. Mean ± s.e.m. *P*-value, two-way ANOVA. **e,** Model. Genome-embedded ribonucleotides (R) can be processed by TOP1 as an alternative to RNase H2-dependent RER. DNA lesions that engage PARP1 (black circles) are formed as a result, and PARP inhibitors induce PARP1 trapping on these TOP1-dependent lesions, causing replication arrest, persistent DNA damage and cell death. See also ED Fig 7, 8, ED Table 1 and Supplementary Table 3.